Defense Threat Reduction Agency
8725 John J. Kingman Road, MS-6201
Fort Belvoir, VA 22060-6201

DTRA-TR-15-26

TECHNICAL REPORT

Detection of Threat Materials Using Terahertz Waveguides and Long Pathlength Terahertz Spectroscopy

May 2015

Grant 11-2210M

Joseph S. Melinger

Prepared by:
Naval Research Laboratory
Electronics Division, Code 6812
4555 Overlook Ave., SW
Washington, DC 20375

DESTRUCTION NOTICE:

Destroy this report when it is no longer needed.
Do not return to sender.

PLEASE NOTIFY THE DEFENSE THREAT REDUCTION AGENCY, ATTN: DTRIAC/ J9STT, 8725 JOHN J. KINGMAN ROAD, MS-6201, FT BELVOIR, VA 22060-6201, IF YOUR ADDRESS IS INCORRECT, IF YOU WISH THAT IT BE DELETED FROM THE DISTRIBUTION LIST, OR IF THE ADDRESSEE IS NO LONGER EMPLOYED BY YOUR ORGANIZATION.

REPORT DOCUMENTATION PAGE

Form Approved
OMB No. 0704-0188

1. REPORT DATE *(DD-MM-YYYY)*	**2. REPORT TYPE**	**3. DATES COVERED** *(From - To)*
00-05-2015	Technical	March 30, 2009 - December 31, 2011

4. TITLE AND SUBTITLE

Detection of Threat Materials Using Terahertz Waveguides and Long Pathlength Terahertz Spectroscopy

5a. CONTRACT NUMBER

5b. GRANT NUMBER
11-2210M

5c. PROGRAM ELEMENT NUMBER

6. AUTHOR(S)
Joseph S. Melinger

5d. PROJECT NUMBER

5e. TASK NUMBER

5f. WORK UNIT NUMBER

7. PERFORMING ORGANIZATION NAME(S) AND ADDRESS(ES)
Naval Research Laboratory
Electronics Division, Code 6812
4555 Overlook Ave., SW
Washington, DC 20375

8. PERFORMING ORGANIZATION REPORT NUMBER

9. SPONSORING / MONITORING AGENCY NAME(S) AND ADDRESS(ES)
Defense Threat Reduction Agency
8725 John J. Kingman Rd
Ft. Belvoir, VA 22060-6201
PM/Allison Lyalikov

10. SPONSOR/MONITOR'S ACRONYM(S)
DTRA

11. SPONSOR/MONITOR'S REPORT NUMBER(S)
DTRA-TR-15-26

12. DISTRIBUTION / AVAILABILITY STATEMENT
Distribution Statement A. Approved for public release; distribution is unlimited.

13. SUPPLEMENTARY NOTES

14. ABSTRACT

This goals of this project are 1) to advance THz waveguide-based methods to measure and fundamentally understand THz vibrational spectra of threat materials, and 2) to create methods to propagate ultrashort THz pulses in the ambient atmosphere of long paths (> 100 meters) for detection of target vapors. Towards the first goal, significant progress was made generalizing the ability of THz waveguide spectroscopy to resolve previously undetected vibrational fingerprint resonances, in understanding the origin of the line narrowing effect at cryogenic temperatures, and in beginning to understand the effect of impurities on THz spectra. Towards the second goal, experimental work successfully demonstrated the propagation of ultrashort THz pulses over a record-long 170 meter path in ambient atmosphere with signal to noise detection as high as 200:1. The transmitted THz pulses were found to undergo reshaping from due to the strong interaction with atmospheric water vapor. The program demonstrated the feasibility of using THz pulses to detect small molecule threat vapors contained in the 170 meter path, through measurement of rotational signatures within the atmospheric transmission windows.

15. SUBJECT TERMS
THz Pulse Waveguide Vapors X-ray

16. SECURITY CLASSIFICATION OF:			**17. LIMITATION OF ABSTRACT**	**18. NUMBER OF PAGES**	**19a. NAME OF RESPONSIBLE PERSON**
a. REPORT	**b. ABSTRACT**	**c. THIS PAGE**	SAR	41	Allison Lyalikov
Unclassified	Unclassified	Unclassified			**19b. TELEPHONE NUMBER** *(include area code)* 703-767-4663

CONVERSION TABLE

Conversion Factors for U.S. Customary to metric (SI) units of measurement.

MULTIPLY →	BY →	TO GET
← TO GET	← BY	← DIVIDE
angstrom	1.000 000 x E -10	meters (m)
atmosphere (normal)	1.013 25 x E +2	kilo pascal (kPa)
bar	1.000 000 x E +2	kilo pascal (kPa)
barn	1.000 000 x E -28	meter^2 (m^2)
British thermal unit (thermochemical)	1.054 350 x E +3	joule (J)
calorie (thermochemical)	4.184 000	joule (J)
cal (thermochemical/cm^2)	4.184 000 x E -2	mega joule/m^2 (MJ/m^2)
curie	3.700 000 x E +1	*giga bacquerel (GBq)
degree (angle)	1.745 329 x E -2	radian (rad)
degree Fahrenheit	$t_k = (t^of + 459.67)/1.8$	degree kelvin (K)
electron volt	1.602 19 x E -19	joule (J)
erg	1.000 000 x E -7	joule (J)
erg/second	1.000 000 x E -7	watt (W)
foot	3.048 000 x E -1	meter (m)
foot-pound-force	1.355 818	joule (J)
gallon (U.S. liquid)	3.785 412 x E -3	meter^3 (m^3)
inch	2.540 000 x E -2	meter (m)
jerk	1.000 000 x E +9	joule (J)
joule/kilogram (J/kg) radiation dose absorbed	1.000 000	Gray (Gy)
kilotons	4.183	terajoules
kip (1000 lbf)	4.448 222 x E +3	newton (N)
kip/$inch^2$ (ksi)	6.894 757 x E +3	kilo pascal (kPa)
ktap	1.000 000 x E +2	newton-second/m^2 ($N-s/m^2$)
micron	1.000 000 x E -6	meter (m)
mil	2.540 000 x E -5	meter (m)
mile (international)	1.609 344 x E +3	meter (m)
ounce	2.834 952 x E -2	kilogram (kg)
pound-force (lbs avoirdupois)	4.448 222	newton (N)
pound-force inch	1.129 848 x E -1	newton-meter (N-m)
pound-force/inch	1.751 268 x E +2	newton/meter (N/m)
pound-force/$foot^2$	4.788 026 x E -2	kilo pascal (kPa)
pound-force/$inch^2$ (psi)	6.894 757	kilo pascal (kPa)
pound-mass (lbm avoirdupois)	4.535 924 x E -1	kilogram (kg)
pound-mass-$foot^2$ (moment of inertia)	4.214 011 x E -2	kilogram-meter^2 ($kg-m^2$)
pound-mass/$foot^3$	1.601 846 x E +1	kilogram-meter^3 (kg/m^3)
rad (radiation dose absorbed)	1.000 000 x E -2	**Gray (Gy)
roentgen	2.579 760 x E -4	coulomb/kilogram (C/kg)
shake	1.000 000 x E -8	second (s)
slug	1.459 390 x E +1	kilogram (kg)
torr (mm Hg, 0^0 C)	1.333 22 x E -1	kilo pascal (kPa)

*The bacquerel (Bq) is the SI unit of radioactivity; 1 Bq = 1 event/s.

**The Gray (GY) is the SI unit of absorbed radiation.

Table of Contents

Title: Detection of Threat Materials Using Terahertz Waveguides and Long Pathlength Terahertz Spectroscopy

Executive Summary: This project represents the collaborative work between the Naval Research Laboratory and Oklahoma State University. The goals of the project are two-fold: 1) to create and fully understand waveguide-based terahertz (THz) measurement methods to improve the resolution, detection sensitivity, and fundamental understanding of THz vibrational fingerprint resonances in threat solids. 2) To create methods to propagate ultrashort THz pulses in the ambient atmosphere over long paths (> 100 meters), understand the effect of the atmosphere on THz pulse propagation, and achieve broadband detection of target vapors through measurement of rotational transitions.

Towards the first goal, the project advanced the ability to produce high crystalline quality films on the surface of a metal parallel plate waveguide (PPWG) in order to resolve the underlying THz vibrational spectra explosives related materials. This ability to resolve underlying fingerprint resonances had not been achieved using standard free space THz methods. Our studies suggest that the degree of crystallinity plays an important role in determining the width of THz vibrational resonances. X-ray diffraction analysis of analyte polycrystalline films formed on the PPWG indicate a smaller degree of inhomogeneous strain in the solid compared to the standard pellet samples, which are traditionally used for THz measurements. The smaller strain in polycrystalline films suppresses inhomogeneous line broadening and leads to a significant line narrowing effect. Potential (deleterious) interactions between the metal waveguide surface and the analyte were probed in systematically. The project demonstrated a remarkable insensitivity of the THz vibrational spectrum to the metal surface (aluminum, copper, and gold) for a variety of analytes. The project also showed that the metal surface can be passivated in a simple way that does not alter the THz spectrum of the analyte. Initial investigations were performed to understand the effect of impurities have on the THz vibrational spectrum of the parent material. At impurity levels between 3-7% (by weight) effects ranged from modest broadening of vibrational lines (due to increased disorder) to more dramatic suppression of vibrational resonances of the parent analyte. Additional research in this area is needed to more fully understand the mechanism by which impurities can alter THz spectra, which could help to define the limits of how THz spectroscopy can be used for materials identification. Finally, to demonstrate potential for increased fundamental understanding the high resolution THz spectra were modeled using solid-state density functional theory carried out by collaborators at Syracuse University. Reasonable agreement between theory and experiment was found which re-enforced the need to fully consider the crystalline environment to accurately predict THz vibrational spectra.

Towards the second goal, the project demonstrated the feasibility to propagate a low power beam of sub-picosecond THz pulses in the ambient atmosphere over a record-long path of 170 meters. THz pulse transmission was characterized under relatively dry ambient conditions (7% relative humidity) and relatively moist ambient conditions (up to 51% relative humidity). The propagating THz pulses undergo reshaping from the approximately 0.5 picosecond input pulse width into an output pulse with a 5 picosecond symmetric pulse with a rapidly oscillating tailing edge extending to 150 picoseconds. The pulse reshaping occurs largely from the interaction with the rotational transitions of water vapor, which strongly absorb portions of the pulse spectrum,

and also cause group velocity dispersion. The THz pulse transmitted 170 meters could be detected with signal to noise of greater than 200:1. The propagated THz pulses were shown to detect small molecule vapors contained within the 170 meter path. This was accomplished through detection of rotational transitions that occur within several atmospheric transmission windows between 0.2 THz and 1.0 THz. The detection was sufficiently stable to resolve rotational band absorptions smaller than about 5%. With improvements to the transmitted THz power and optimization of the THz pulse bandwidth it's anticipated that detection sensitivity can be further improved.

The project supported the activities of Dr. Joseph S. Melinger (NRL), Professor Daniel Grischkowsky (OKState), Dr. Ani Khachatrian (Postdoctoral Associate at NRL), and graduate students from OKState: Sree Harsha Srikantaiah, Yihong Yang, and Mahboubeh Mandeghar. Portions of the work carried out in this project contributed to the Ph.D. thesis of Sree Harsha Srikantaiah, "Engineering Metal Parallel Plate Waveguides As a 2-D Plane for High Resolution THz Time Domain Spectroscopy," which can be found at the website: http://utol.ecen.ceat.okstate.edu/PhDTheses.htm.

Personnel Supported:

Government: Dr. Joseph S. Melinger, Naval Research Laboratory

Academia: Professor Daniel Grischkowsky, Oklahoma State University

Postdoctoral Associate: Dr. Ani Khachatrian, Naval Research Laboratory

Graduate Students (Oklahoma State University): Srikantaiah Sree Harsha, Yihong Yang, Mahboubeh Mandeghar.

Journal Publications:

1. "Temperature dependent characterization of THz vibrations of explosives and related threat materials," Joseph S. Melinger, S. Sree Harsha, N. Laman and D. Grischkowsky, Optics Express, 18, 27238-27250, (2010).

2. "Solid-state density functional theory investigation of the THz spectra of the structural Isomers 1,2 Dicyanobenzene and 1,3-Dicyanobenzene," Keith C. Oppenheim, Timothy M. Korter, Joseph S. Melinger, and D. Grischkowsky, J. Phys. Chem. A 2010, 114, 12513-12521, (2010).

3. "Measurement of the transmission of the atmosphere from 0.2 to 2 THz ," Yihong Yang, Alisha Shutler, and D. Grischkowsky, Optics Express, 19, 8830-8838, (2011).

4. "Broadband THz Pulse Transmission Through the Atmosphere", Yihong Yang, Mahboubeh Mandeghar, and Daniel R. Grischkowsky, IEEE Trans. Terahertz Science and Technology, 1, No. 1, 264-273, (2011).

5. "Substrate independence of THz vibrational modes of polycrystalline thin films of molecular solids in waveguide THz-TDS," S. Sree Harsha, Joseph. S. Melinger, S. B. Qadri and D. Grischkowsky, J. of Appl. Phys. Lett., 111, 023105, (2012).

6. "THz detection of small molecule vapors in the atmospheric transmission windows," Joseph. S. Melinger, Yihong Yang, Mahboubeh Mandeghar and D. Grischkowsky, Optics Express, 20, pp.6788-6807, (2012).

7. “Waveguide terahertz time-domain spectroscopy of ammonium nitrate polycrystalline films,” A. Khachatrian, Joseph S. Melinger, and S.B. Qadri, J. Appl. Phys. 111, 093103 (2012).

Conference Proceedings:

1. ”Broadband THz Detection of Small-Molecule Vapors in the Atmospheric Transparency Windows,” Joseph S. Melinger, Yihong Yang, M. Mandeghar, and Daniel Grischkowsky,

36th International Conference on Infrared, Millimeter, and Terahertz Waves (IRMMW-THz), 2-7 October 2011, Houston, TX. DOI: 10.1109/irmmw-THz.2011.6104789. Pages 1-3.

2. "High resolution terahertz spectroscopy of ammonium and potassium nitrate films," A. Khachatrian, S. Qadri, and Joseph S. Melinger 36th International Conference on Infrared, Millimeter, and Terahertz Waves (IRMMW-THz), 2-7 October 2011, Houston, TX. DOI:10.1109/irmmw-THz.2011.6105219. Pages 1-2.

3. "Long path THz detection of small molecule vapors in the atmospheric transparency windows," J. S. Melinger, A. Shutler, Y. Yang, and D. Grischkowsky, Conference on Lasers and Electro-Optics CLEO-2011 OSA Technical Digest (Optical Society of America, Washington, D.C., 2011), CThEE7.

4. "Guided wave terahertz characterization of fingerprint lines in threat materials," Joseph S. Melinger, S. Sree Harsha, N. Laman, and D. Grischkowsky, Proc. SPIE 7671, 76710H (2010)

Presentations:

1. "Broadband THz Detection of Small-Molecule Vapors in the Atmospheric Transparency Windows," Joseph S. Melinger, Yihong Yang, M. Mandeghar, and Daniel Grischkowsky, 36th International Conference on Infrared, Millimeter, and Terahertz Waves (IRMMW-THz), 2-7 October 2011, Houston, TX. **Oral. Invited Keynote**

2. "High resolution terahertz spectroscopy of ammonium and potassium nitrate films," A. Khachatrian, S. Qadri, and Joseph S. Melinger 36th International Conference on Infrared, Millimeter, and Terahertz Waves (IRMMW-THz), 2-7 October 2011, Houston, TX. **Poster**

3. "Long Path THz Detection of Small Molecule Vapors in the Atmospheric Transparency Windows ," J.S. Melinger, Y. Yang, A. Shutler, and D. Grischkowsky, Conference on Lasers and Electro optics, 1-6 May, 2011 Baltimore, MD. **Oral**

4. "High resolution characterization and simulation of terahertz vibrations of explosives and related threat materials," J.S. Melinger, K. Oppenheim, and T.M. Korter, International Workshop on Optical Terahertz Science and Technology, March 14, 2011 Santa Barbara, CA. **Oral**

5. "Substrate independence of THz vibrational modes of polycrystalline thin films of molecular solids in waveguide THz-TDS," S. Sree Harsha, D. Grischkowsky, and J.S. Melinger, International Workshop on Optical Terahertz Science and Technology, March 14, 2011 Santa Barbara, CA. **Oral**

6. "Guided wave terahertz spectroscopy," J.S. Melinger, Physics Department Seminar, University of Maryland at Baltimore, April 21, 2010. **Oral**

7. “Guided wave terahertz characterization of fingerprint lines in threat materials,” J.S. Melinger, SPIE Conference, Defense, Security and Sensing, April 5-9, Orlando, FL (2010). **Oral, Invited**

8. “High Resolution Characterization of Explosives Materials using Waveguide THz Time-Domain Spectroscopy,” J.S. Melinger, Pacifichem 2010, Security, Dec.18, 2010, Honolulu, HI. **Oral**

9. “Guided-wave terahertz spectroscopy,” J.S. Melinger, The Southeastern Regional Universities 6th Terahertz Applications Symposium, American Academy of Science, Jun 11-13,Washington DC (2009). **Oral**.

Technical Summary:

1. THz Waveguide Spectroscopy

Introduction: Terahertz (THz) spectroscopy (0.1 THz – 10 THz; 0.3 cm^{-1} – 333 cm^{-1}) has become an important tool for studying the low frequency vibrational properties of molecules in the condensed phase. In addition to fundamental studies, THz spectroscopy has also shown strong potential for security applications related to the detection of threat materials [1,2]. The ability to use THz spectroscopy for this application will be enhanced by obtaining a deeper fundamental understanding of THz vibrational spectra.
To date, there have been several investigations of the far infrared properties of explosives solids and their related derivatives and simulation materials [3–7]. These studies have shown that many of the explosive solids have distinct vibrational absorption features at room temperature that can be used for characterization and identification. However, these absorption features tend to be rather broad and overlapping with Q factors ($f/\Delta f$) often << 10. The broad absorption features are a consequence of the broadening of the underlying individual THz resonances due to homogeneous and inhomogeneous line broadening mechanisms. The resolution of the underlying THz resonances of an explosives solid is a challenging problem and is necessary to achieve a full understanding of the THz properties of explosives, and to make rational use of database THz spectra for detection applications.

To demonstrate significantly higher spectral resolution and ability to resolve closely spaced lines we use an experimental approach based on a parallel plate waveguide (PPWG) with a sub-wavelength gap between the two plates. The technique is called waveguide terahertz time-domain spectroscopy (THz-TDS). Here, a polycrystalline film of a target analyte is formed on one of the inner surfaces of the waveguide plate. The confinement of THz waves ($\lambda/6$ for a typical 50 micron gap) together with a long interaction pathlength (~2-3 cm) allows the THz response of the film to be measured in a sensitive manner over a broad bandwidth from 0.2 THz – 4 THz. A key finding is that using relatively simple film formation methods it is possible to form a highly crystalline quality thin film, which minimizes inhomogeneous line broadening that plagues traditional THz sample preparation methods such as pellet formation. We demonstrate that the high crystalline quality films formed in our waveguide approach leads to the resolution of fingerprint lines in threat solids which are not observed in the conventional free space THz spectroscopy of corresponding pellet samples. At cryogenic temperatures, our method produces vibrational linewidths as narrow as our instrument window, which is approximately 7 GHz (0.21 cm^{-1}). We show that the high resolution measurements can be used as rigorous input to test theoretical models used to simulate THz spectra.

In the film formation process it's important to test for potential interactions from the metal surface of the PPWG that might alter the THz spectrum of the parent analyte. We show that there can be a remarkable insensitivity to the substrate metal (aluminum, copper, and gold). Further, we also show it is possible to passivate the metal surface with a dielectric layer in a way that does not alter the THz spectrum of the analyte film.

The high resolution from waveguide THz-TDS is useful to study how impurities can affect the THz spectrum of a solid film. In this project we performed preliminary experiments whereby small amounts of an impurity were introduced into the lattice of the parent material deposited on the PPWG surface. The observed effects ranged from moderate line broadening of the vibrational resonances, to a more severe suppression of some of the individual vibrational resonances. A fundamental understanding of how impurities affect THz spectra is important for potential fingerprinting applications.

Experimental Methods: The measurement method for waveguide THz-TDS is outlined in Fig. 1 and uses well established ultrafast optoelectronic techniques to generate and detect sub-picosecond THz pulses [8]. For measurements at low temperature the analyte materials can cooled to near 10 K using a two-stage He cryocooler or cryostat.

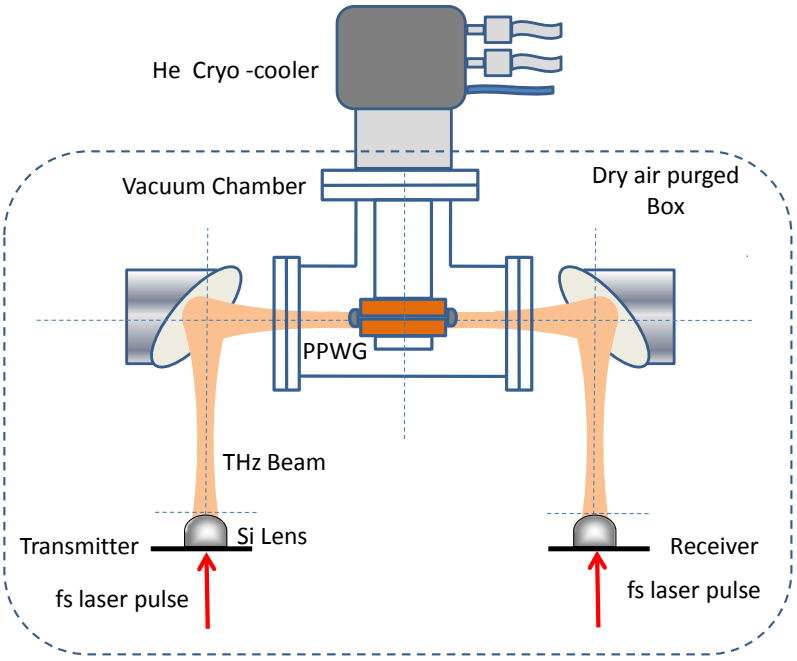

Fig. 1 Schematic of the waveguide THz-TDS apparatus.

THz pulses are coupled into and out of a PPWG with a 50 micron gap using plano-cylindrical high resistivity Si lenses at the entrance and exit faces of the assembly. A schematic of the coupling into the PPWG is shown in Fig. 2. A picture of an aluminum PPWG used for sample measurements is shown in Fig. 3. The waveguide assembly is fabricated using standard machining methods and with standard tolerances. The typical dimension of a waveguide plate is 30 mm (length) x 27.9 mm (width) x 9.7 mm (height). The waveguide plates can also be fabricated from copper or gold-coated copper. The polarization of the THz field is perpendicular to the waveguide surface. The spectral resolution is 6.7 GHz which corresponds to 150 picosecond scan lengths. Typically, between two and eight temporal scans were averaged to improve the signal to noise ratio.

To recover the absorbance spectrum, which includes any broadband background absorption, it is necessary to measure the reference spectral amplitude for the empty PPWG. The amplitude absorbance is then obtained as –ln(Asig/Aref), where Asig and Aref are the spectral amplitudes for the PPWG containing the layer and the empty PPWG, respectively. The reference spectral amplitude is estimated from the film spectral amplitude by choosing points outside the absorption lines and then fitting the points with a smooth function, which includes any broadband absorption. While this method yields only approximate intensities, and not the broadband absorption, it is possible to extract line frequencies and linewidths.

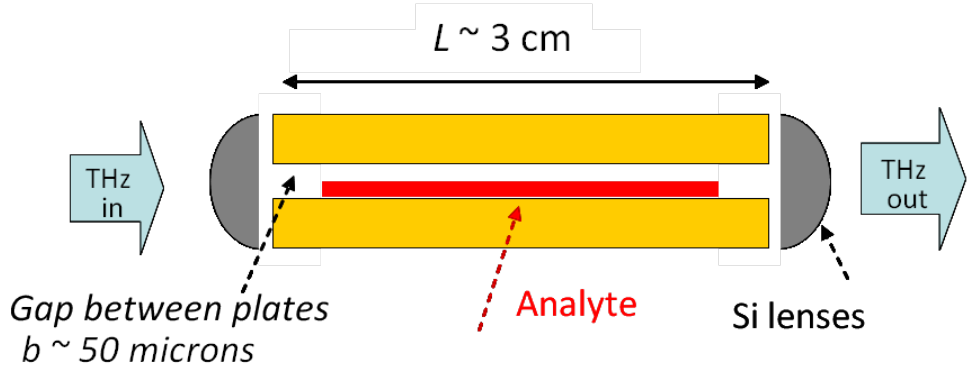

Fig. 2. Schematic of coupling into the metal parallel plate waveguide using plano-cylindrical Si lenses

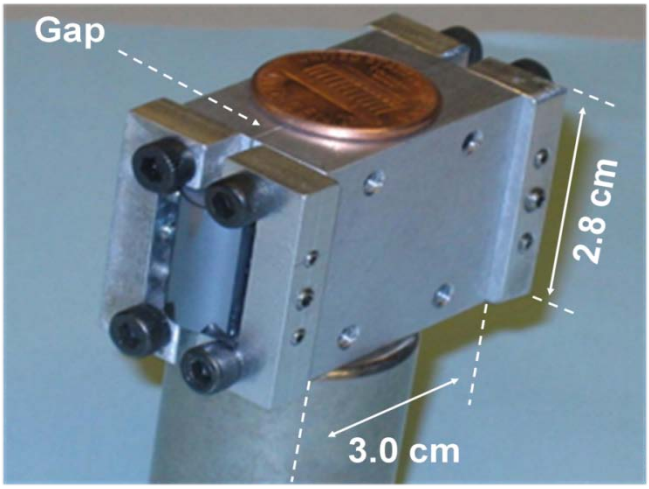

Fig. 3. Picture of a parallel plate waveguide fabricated entirely from aluminum. The front face shows one of two plano-cylindrical high resistivity Si lenses used to couple THz waves into and out of the 50 micron gap.

The sample preparation procedure is outlined in Fig. 4. Here the inner surface of the PPWG was cleansed with solvent (such as acetone) and then plasma cleaned. Solutions of analyte in an appropriate solvent (organic or aqueous) were concentrated to approximately 2-4 milligrams/milliliter. Approximately 100-200 microliters of solution were dropped on the PPWG surface. After evaporation, the relatively thick edges of the film around its perimeter were swabbed away using a solvent soaked swab. This typically produced a film footprint about 10-15 millimeters in width and 10-20 millimeters in length. The morphologies of the microcrystals were characterized under a microscope and recorded as optical micrographs. X-ray diffraction was used as an analytical tool to confirm the integrity and crystallinity of the microcrystals on

the waveguide surface, check for polymorphism, and to determine the orientation of the microcrystals on the surface. It's worth noting that the high sensitivity of the 50 μm gap PPWG requires only about 1% of the sample mass typically used in free space THz characterization.

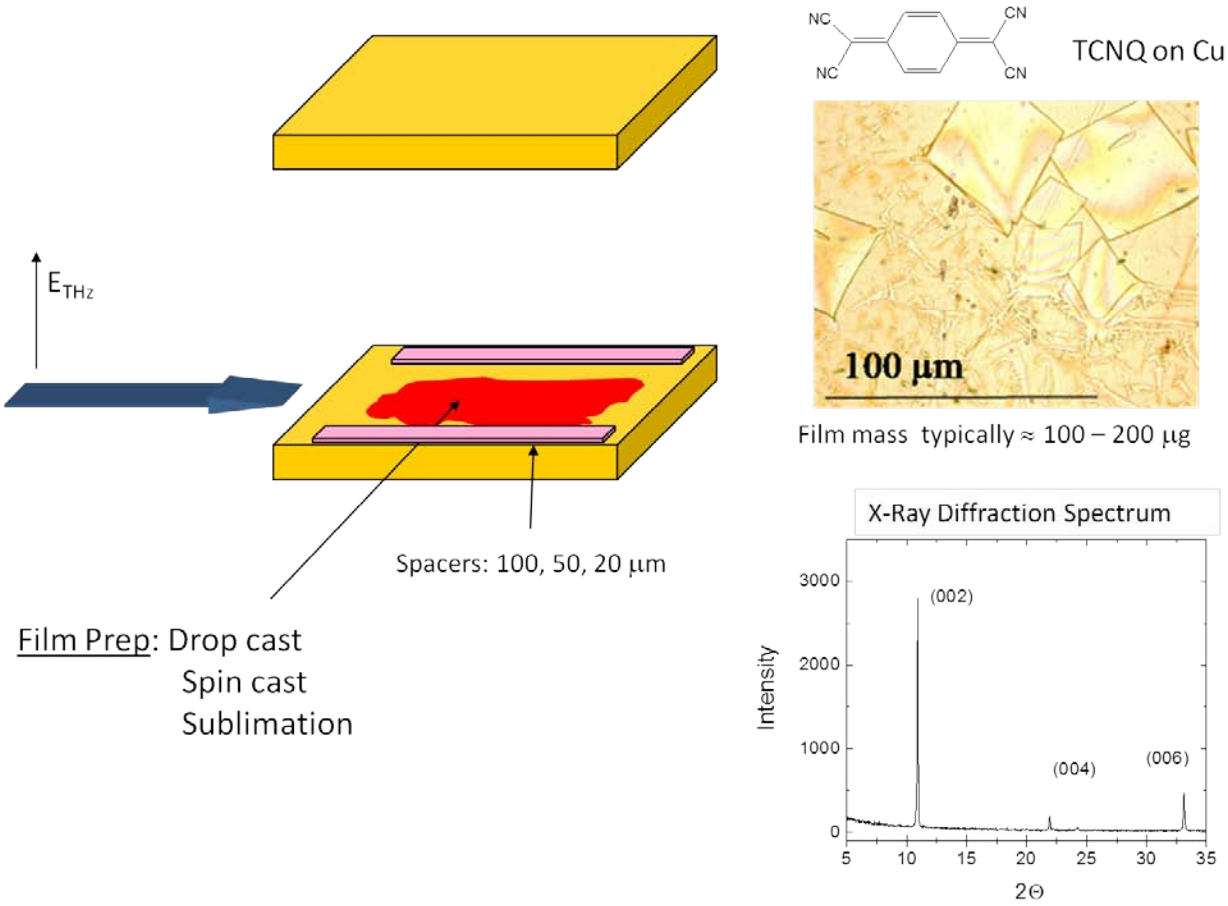

Fig 4. Schematic of methods used for thin film preparation on the PPWG surface and subsequent analytical characterization.

Results:

Waveguide Spectroscopy: Our first experimental demonstration of the line narrowing power of waveguide THz-TDS is for the explosive pentaerythritol tetranitrate, or PETN. The most stable form of the explosive PETN crystallizes in the orthorhombic space group P-421c with Z = 2 molecules per unit cell [9]. In this case simple considerations predict 6Z-3, or nine phonon modes, and 3N-6 (N = 29 atoms for PETN) or 81 intramolecular modes. The phonon modes are expected to occur in the THz region, as well as the low frequency intramolecular modes. Therefore a complex spectrum is anticipated. In the range between 0.2 THz and 3.0 THz there have been several free space THz spectroscopy measurements made for PETN in a mixed pellet form [3,5,6], where the analyte material is ground into a fine powder and mixed with a transparent matrix material, such as polyethylene powder, and pressed under high pressure. For comparison, an example taken from Ref. 3 is shown in Fig. 5, left upper panel. Here, at room temperature, the PETN pellet spectrum shows two prominent broad absorption features near 1.9 THz and 2.8 THz with FWHM linewidths greater than 200 GHz. At the low temperature of 4 K the absorption features shift to higher frequency, but only show a modest narrowing. A more complex underlying spectrum is only suggested, but not resolved. A PETN layer was formed on an Au-coated PPWG surface by drop casting from a 2 mg/ml solution in acetonitrile. The estimated mass is 150 μg. PETN on Au forms a dendritic type of morphology as shown in the optical micrograph of Fig.5, right upper panel. An equivalent homogeneous layer thickness of approximately 400 nanometers is estimated by using the density of PETN (1.77 g/cm3), and considering that the estimated mass of 150 μg is spread over an area of approximately 2 cm^2. X-ray diffraction (Fig. 5, right lower panel) confirmed the integrity of the PETN microcrystals. The appearance of several diffraction lines could be assigned to crystalline planes of PETN confirming that the structure of the PETN film has not been altered by the waveguide surface. To contrast the standard pellet measurement, the 12 K measurement in Fig. 5 (left lower panel) shows a highly resolved underlying THz vibrational spectrum consisting of a series of eleven lines between 1.0 THz and 3.5 THz [10]. The sharp lines of the PETN layer can be correlated with those of the previous free space THz measurements of PETN pellets [3] (both at room temperature and 4 K). For example, the broad absorption feature near 1.9 THz undergoes a blue shift of 0.21 THz (7.0 cm^{-1}) upon cooling to 12 K, and splits into four lines that include the relatively strong doublet of lines at 2.234 THz and 2.349 THz, and the weaker lines at 2.14 THz and 2.555 THz. In addition, the broad absorption feature of the PETN pellet near 2.8 THz splits into five lines for the PETN layer at 12 K. The prominent line near 2.24 THz has a FWHM linewidth of about 30 GHz in the 12 K spectrum. This represents about a factor of about 7 in line narrowing when compared to ~200 GHz linewidth of the room temperature line at 2.01 THz. The high sensitivity and high spectral resolution of the measurement are highlighted by the observation of weak lines at 1.101 THz and 1.710 THz. These lines have FWHM linewidths of 7 GHz and 10 GHz, respectively. We mention that we observed essentially the same line frequencies and relative intensities for PETN films on an aluminum PPWG surface.

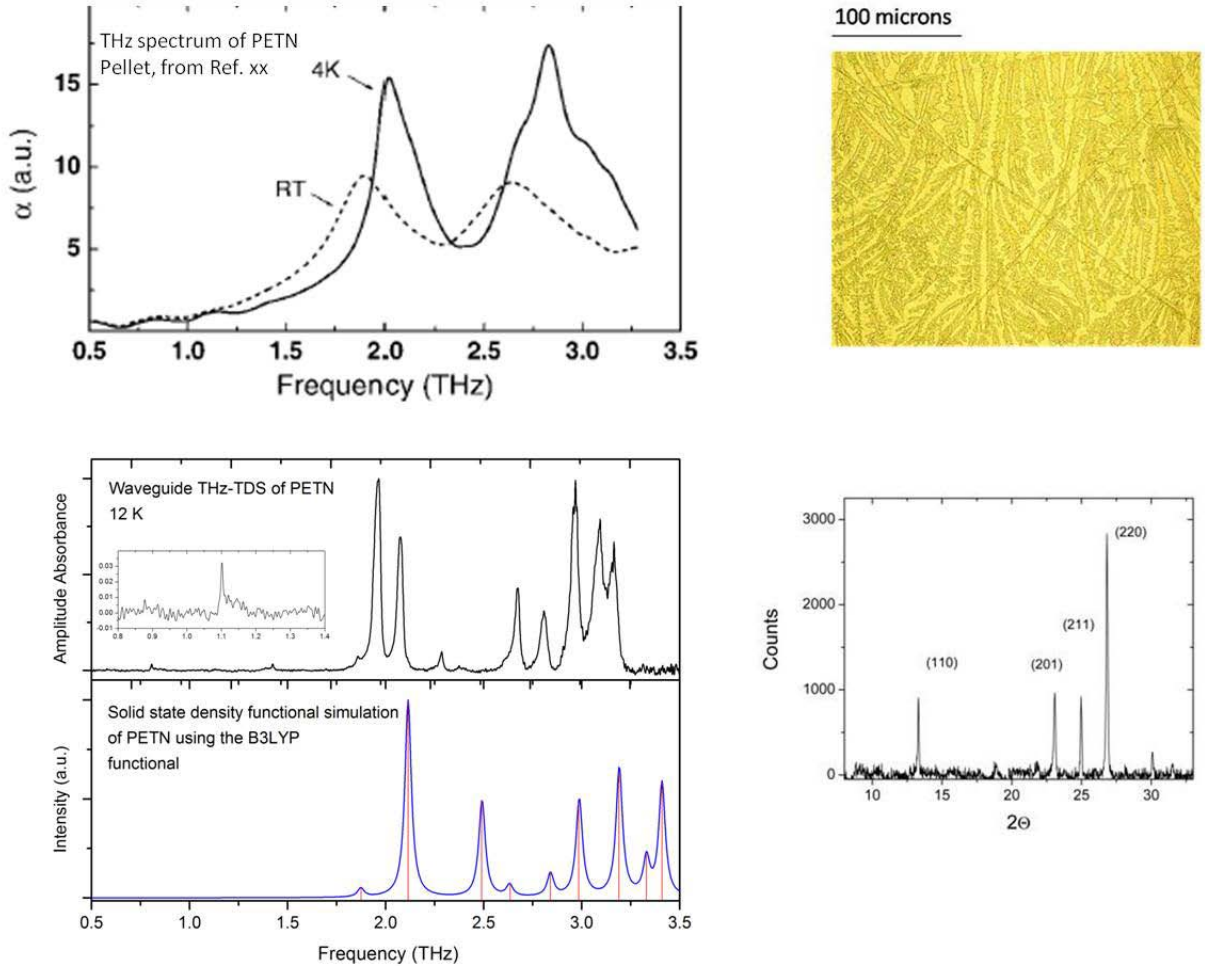

Fig. 5. Left upper panel: Room temperature and low temperature THz spectrum of a PETN sample in conventional pellet form (taken from reference 3). Left middle panel: High resolution waveguide THz-TDS of PETN film on a gold-coated PPWG surface. Left lower panel: Solid state density functional simulation of the PETN THz spectrum using the B3LYP functional. Right upper panel: Optical micrograph of the PETN film on the gold-coated PPWG plate. Right lower panel: X-ray diffraction pattern of PETN film showing lines that are correlated with planes of the PETN crystal (P-421c).

Other demonstrations of high resolution waveguide THz-TDS were achieved for threat solids and simulant threat solids, including the materials 4-amino-dinitrotoluene (4A-DNT), octahydro-1,3,5,7-tetranitro-1,3,5,7-tetrazocine (HMX), and ammonium nitrate [10]. In each case the waveguide THz-TDS method produced a highly resolved underlying THz vibrational spectrum with vibrational resonances of similar linewidth (at cryogenic temperature) to those observed in PETN. In the case of 4A-DNT the sensitivity and resolution were high enough to unambiguously observe a polymorphic transition from an orthorhombic unit cell ($Cmc2_1$) to a triclinic unit cell via a sudden shift of a THz mode frequency near 180 K.

Theoretical Modeling: From a fundamental viewpoint an important use for high resolution waveguide THz-TDS is that the narrow linewidths and precisely specified line frequencies serve as rigorous input to test theoretical models that predict THz vibrational spectra. Solid-state THz spectra are particularly challenging to model, since the spectra are composed of intramolecular

and intermolecular vibrations as well as combinations of these motions. Any successful theoretical method must be able to account for all types of motions simultaneously. A major challenge for the theory is to accurately incorporate the long range intermolecular interactions that are important in molecular crystals. The modeling of our high resolution THz spectra was performed by the group of Professor Tim Korter at the Syracuse University Department of Chemistry. As a first example, the high resolution THz spectrum of the crystalline solid 1,2 dicyanobenzene (12DCB) was modeled using solid state density functional theory. All calculations in this work were performed starting with the measured crystal lattice parameters studies and applying periodic boundary conditions.

Figure 6 shows a comparison of the experimental 12DCB THz spectrum measured at 12 K and the predicted THz spectrum using the B3LYP hybrid functional [11]. The simulated spectrum includes a 2:1 ratio of the Z=4 (P21/c) and Z=2 (Pmn21) polymorphs, which is consistent with x-ray analysis of the 12DCB film. Each of the simulated line frequencies can be correlated with an intermolecular vibration of the unit cells of the individual polymorphs [11]. No mode mixing between intermolecular and intramolecular vibrations are predicted for 12DCB because the lowest frequency intramolecular modes fall at higher frequencies than the intermolecular vibrations (and also at frequencies beyond measured in the experiment). The simulation show reasonable agreement with the experimental spectrum in terms of the observed absorption frequencies and relative intensities. However, it is noted that the solid state density functional simulation for PETN shown in Fig. 5 shows better agreement with experiment. This may be due to the presence of weak hydrogen bonding interaction in the PETN crystal, which are absent in the case of 12DCB. It is anticipated that for 12DCB, and similar van der Waals type molecular crystals, better agreement between theory and experiment will result from more accurate incorporation of long range dispersion forces.

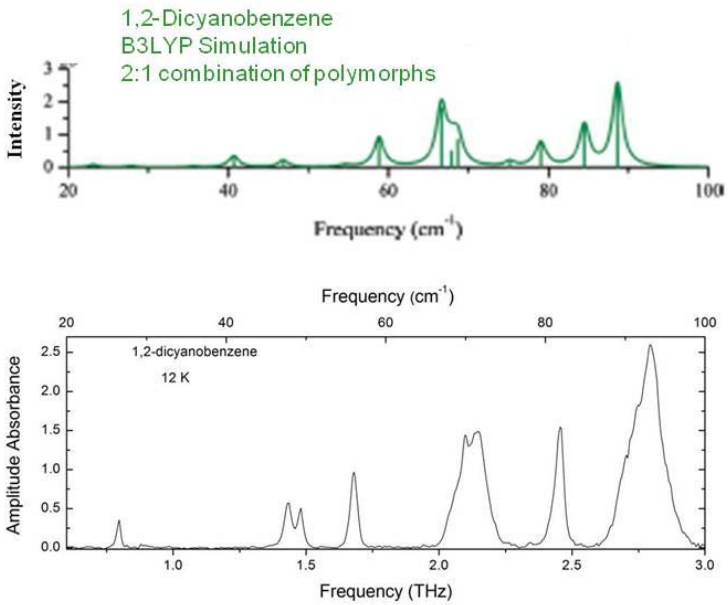

Fig. 6. Top: Simulated THz spectrum of 12DCB from solid state density functional theory. Bottom: Experimental waveguide THz-TDS spectrum of 12DCB measured at 12 K

Origin of Line Narrowing in Waveguide THz-TDS: We conducted experiments to help determine the origin of the significantly narrower vibrational lineshapes of waveguide THz-TDS compared to standard THz measurements of pressed pellet samples. There are at least two possible mechanisms. The first is related to the thermal contact of the sample with the cold finger of the cooling apparatus. In this cooling configuration the metal PPWG makes good thermal contact with the cold finger and therefore the thin film on the waveguide surface rapidly reaches a uniform temperature close to that of the cold finger. However, a pressed pellet sample has relatively low thermal conductivity and therefore will take significantly longer to reach the temperature of the cold finger. If the pellet sample does not reach the same low temperature as the film sample, then the pellet sample will contain a larger degree of *homogeneous line broadening*, and therefore will display broader vibrational lineshapes. A second mechanism has to do with differing degrees of crystallinity in the polycrystalline sample on the waveguide surface and the pellet sample. In the case of the film formed on the PPWG by drop casting the microcrystals are anticipated to form under relatively low strain conditions, and therefore exhibit high crystallinity (relatively low density of defects). In contrast, to form a suitable pellet sample, the analyte solid is first ground into a fine powder and then pressed under several tons of pressure with a matrix material to form the pellet. For sufficiently soft solids, such as many organics, it's possible that the standard pellet preparation introduces significant strain and defects in the form of *inhomogeneous line broadening*. To better assess the effects of temperature vs sample preparation we first compared measurements of THz lineshapes for a given material in the form of a film in waveguide THz-TDS and in the form of a mixed pellet sample. The measurements were performed at cryogenic temperature as close to 77 K as possible. The two samples were then analyzed by x-ray diffraction in the θ–2θ configuration. Here, particular attention was paid to the width of the diffraction peaks as a function of diffraction angle, which contains information on lattice strain. For example, an increasing width of the diffraction peaks for increasing diffraction angle is suggestive of strain broadening through a Williamson-Hall analysis [12].

The organic solid tetracyanoquinodimethane (TCNQ) was used as a test material. A thin film sample was prepared on an aluminum PPWG surface by drop casting from a 2 mg/ml solution of TCNQ in acetone. A mixed TCNQ-polyethylene pellet sample was prepared by thoroughly grinding the small TCNQ crystals (Aldrich, 98%) into a fine powder and then thoroughly mixing about 30 mg of ground TCNQ powder with about 300 mg of polyethylene powder (Micropowders). The mixture was then pressed under 4 tons of pressure into 1-2 mm thick pellet samples (1 cm diameter). To estimate the temperature that the pellet sample reached in a liquid nitrogen cooled cryostat, a small hole was formed in the center of one of the pellet samples and mounted a thermocouple sensor directly to the pellet surface. The pellet was then placed in its sample mount and attached to the cold finger of the cryostat. The cryostat was cooled to 79 K (at the cold finger) and the pellet temperature monitored over the course of several hours until no further temperature changes were observed. Over several different runs we the pellet samples consistently cooled to an equilibrium temperature of 82-83 K, over a time of about three hours. Therefore, if sufficient cooling time is used it is possible for the pellet to approach the cold finger temperature.

A comparison of the THz vibrational spectra for the TCNQ film at 79 K, measured using waveguide THz-TDS, and the mixed TCNQ pellet at 82 K, measured using free space THz-TDS

is shown in Fig. 7. The linewidth of lowest frequency mode near 1.3 THz is narrower for the film sample by approximately a factor of two. The higher frequency mode near 2 THz is also narrower for the film sample, though by a smaller factor of about 1.5. Interestingly the blue shift of the line frequency for the cooled pellet sample (from the room temperature line frequency) is slightly larger for the pellet sample. Given that the two samples reach rather similar temperatures, the experiment suggests that the significantly larger linewidths for the pellet sample is related to inhomogeneous broadening.

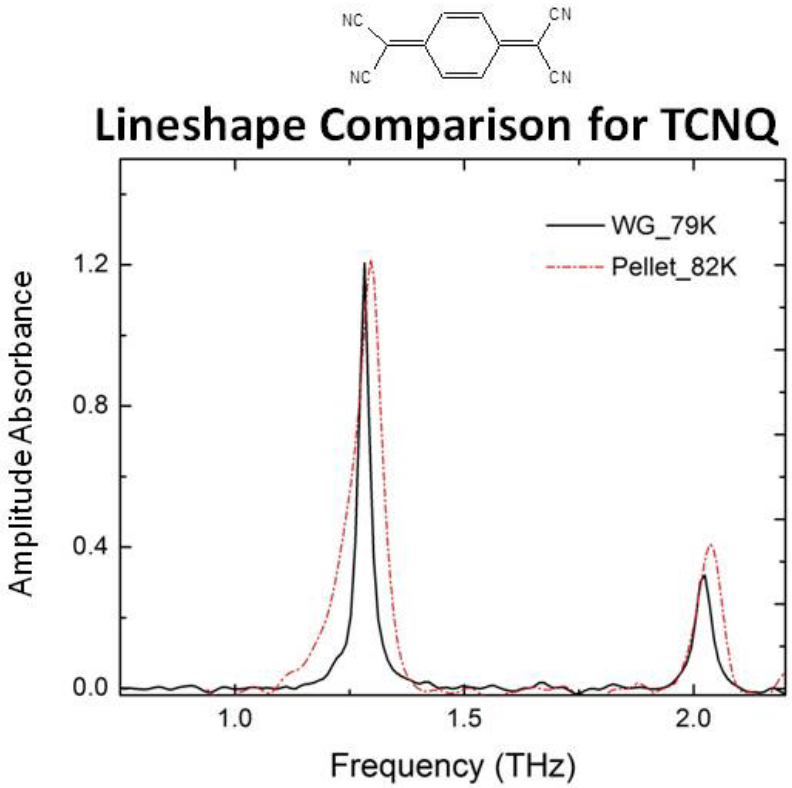

Fig. 7. Comparison of THz spectra for a TCNQ polycrystalline film in a PPWG at 79 K (black curve) and a mixed TCNQ/polyethylene pellet sample at 82 K (red curve).

To determined in a qualitative manner the potential importance of inhomogeneous broadening from strain effects we performed diffraction experiments on the waveguide TCNQ film and TCNQ mixed pellet sample using the Williamson-Hall analysis mentioned above. This approach relies on the broadening of a diffraction peak produced by crystallite size and by inhomogeneous strain. The Williamson-Hall equation may be written as

$$\frac{\beta \cos\theta}{\lambda} = \frac{C\varepsilon \sin\theta}{\lambda} + \frac{K}{L}$$

Where β is the FWHM width of the diffraction peak (minus the instrument width), θ is the diffraction angle (in radians), $C\varepsilon$ is related to the inhomogeneous strain broadening, λ is the wavelength, L is the size of the crystallite, and K is a constant taken to be close to 1. By plotting

$\beta\cos\theta/\lambda$ vs $\sin\theta/\lambda$ one can qualitatively check for a strain component from the slope ($C\varepsilon$), and the size component from the intercept (K/L). This is shown qualitatively in Fig. 7, which indicates a significantly broader diffraction width for the (002) peak of the pellet sample (Fig. 7, left panel). In Fig. 7 (right panel) the broadening of the diffraction peaks for the TCNQ film showed a nearly zero slope, implying a relatively small degree of inhomogeneous strain, compared to the pressed TCNQ pellet, which showed a significant positive slope, implying a significantly higher degree of inhomogeneous strain. The measurements of Fig. 7 and Fig. 8, taken together, suggests that inhomogeneous broadening (most likely from strain effects induced by pellet preparation) plays a strong role in broadening the THz spectra of traditional pellet samples. At cryogenic temperatures well below 77 K we anticipate that it will become more difficult for the pellet sample to reach the temperature of the cold finger. At temperatures near 10 K it is possible the broader spectra of traditional pellets are more strongly related to a non-uniform temperature across the pellet sample.

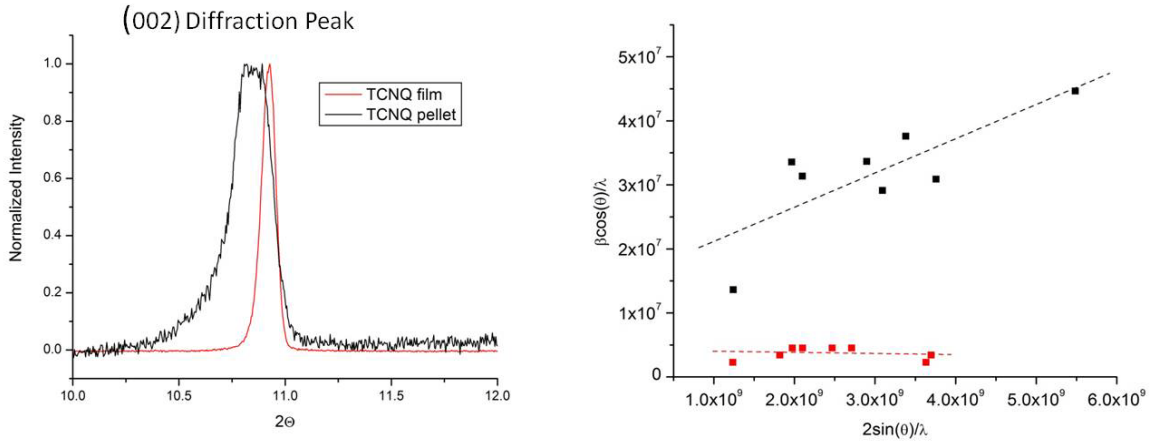

Fig. 8. Left panel: Comparison of the (002) diffraction peak for mixed pellet and film samples of TCNQ. Williamson-Hall plot of the TCNQ film (red data points) and the TCNQ pellet sample (black data points). The X-ray radiation was 1.5418 Angstroms. The dashed lines are linear fits to the data points.

We note that results similar to Fig. 8 were obtained for other crystalline analyte materials, including benzoic acid and derivatives.

Independence of THz Spectra to the Metal Surface: An important fundamental issue is the potential influence of the metal waveguide surface on the THz spectrum of the analyte film that crystallizes on the surface. This issue is crucial to fully understand for any potential applications of waveguide THz-TDS to identification of threat materials. One possibility is a potential for chemical interactions between the metal surface and the analyte, which can range from a chemical reaction that alters the chemical structure of the analyte, or complex formation where metal ions incorporate into the lattice of the analyte. In each of these cases the resulting THz spectrum would be drastically different from that of the native analyte. In fact, we have observed complex formation in the case amino acid films that form from aqueous solution on a copper waveguide surface, which results in an altered THz spectrum through the incorporation of copper into the solid amino acid matrix [13]. A second possibility is a physical interaction at the interface between the metal surface and the analyte film. If such interactions are significant then

there will be additional vibrational modes that involve the correlated motion of both the analyte and the metal. However, if these modes are confined to the interfacial region then the contribution to the observed THz spectrum may not be resolvable above the noise floor.

To test for significant interactions between the metal surface and analyte we conducted a systematic experiment whereby the same analyte film was crystallized on three different metal waveguide surfaces, Cu, Al, and Au, and two passivated metal surfaces, consisting of a thin (2 micron) layer of the polymer mylar (polyethylene terephthalate) covering a Cu waveguide surface, and a monolayer of 11-undecanethiol, which self assembles onto a Au surface. For each surface a polycrystalline film of salicyclic acid (derivative of aspirin) was formed by the drop casting method from acetone solution. Salicylic acid was chosen as a test material because its THz spectrum consists of a series of well resolved lines which simplifies the analysis. The observed waveguide THz-TDS spectra (measured at 12 K) showed a remarkable independence to the different metal surfaces and passivated metal surfaces [14,15]. X-ray diffraction analysis of the films showed the same diffraction peaks for each film and therefore ruled out the presence of physical or chemical interactions that would cause a change in the crystallographic properties of the films. This demonstration showed that if physical interactions between the metal surface and analyte film exist then they are confined to the interfacial region and are not detected with the current level of signal to noise. Furthermore, the experiment demonstrated the potential to use simple passivation methods to suppress such interactions if they occur in other cases.

Effects of Impurities on THz Spectra: To date, most measurements of THz spectra have been made using relatively pure materials. However, for potential applications where THz spectroscopy is used to identify threat solids it is important to have an understanding of how impurities affect the vibrational resonances. This is particularly important because suspected threat materials found in the field are likely to be significantly less pure than the materials used for study in the laboratory. In addition, because THz vibrational modes typically involve a large degree of intermolecular vibrational motion (phonons) they will tend to be more sensitive to external effects, such as impurities, degradation, and aging of the crystalline structure. For threat materials such as explosives there have been relatively few studies of how impurities affect the THz resonances. In this project, using the higher spectral resolution possible with waveguide THz-TDS we have begun to study in a systematic way the effects of impurities on the THz spectrum of a parent material. Experimental measurements were made where an impurity molecule at a specific concentration was incorporated into the film of a parent analyte. To make films doped with an impurity we used the drop casting method where small amounts of the impurity material (3-6% by weight) were added to host solution containing the parent analyte. Upon solvent evaporation the film that forms on the waveguide surface contains the impurity material. In the first case, the parent material was ammonium nitrate (AN) and potassium nitrate (KN) was introduced as an impurity. The potassium ion radius is only slightly larger than the ammonium ion radius, thus in a mixed crystal system the potassium ion can replace the ammonium ion. In the second case the parent material is the explosive-related material 2,4 dinitrotoluene (24DNT) and the impurity is the isomer 2,6-dinitrotoluene (26DNT). Both 24DNT and 26DNT are byproducts of TNT synthesis.

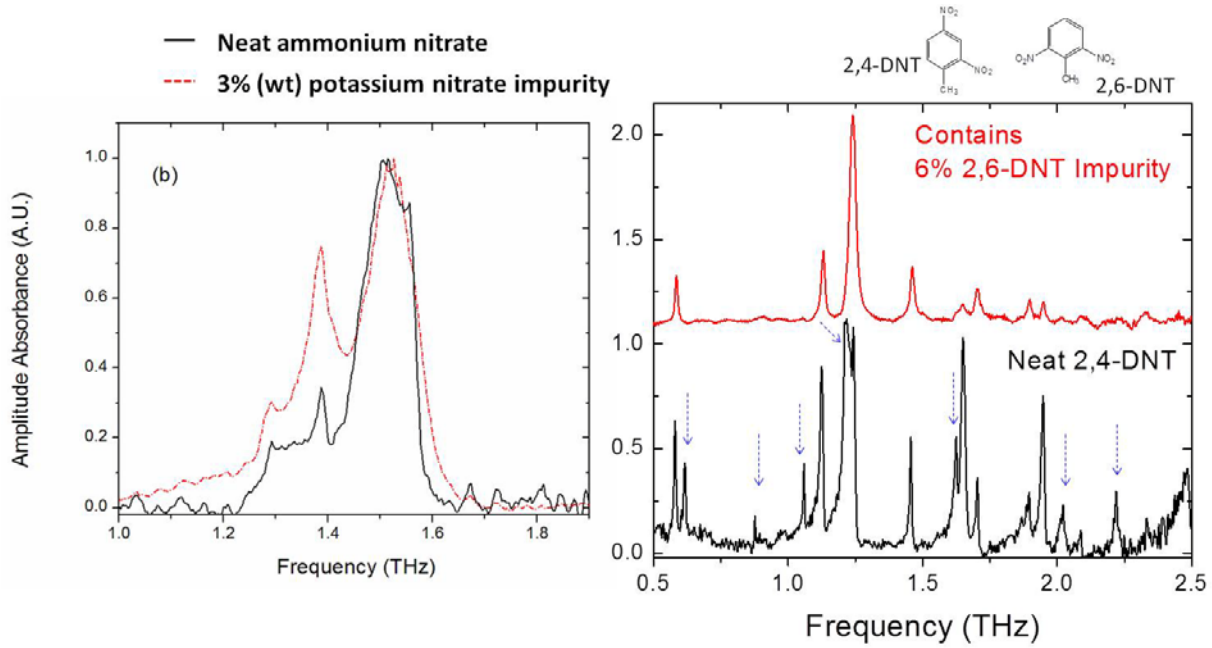

Fig. 9. Left: The black curve is the waveguide THz-TDS spectrum of neat AN and the red curve is the corresponding THz spectrum of AN doped with 3% by weight KN. The ammonium nitrate vibrational resonances are noticeably broadened by the addition of the impurity. The measurement is made at 5 K. Right: The black curve is the waveguide THz-TDS spectrum of neat 24DNT and the red curve (displaced upwards for clarity) is the waveguide THz-TDS spectrum of the parent film containing 6% by weight of 26DNT as an impurity. The measurement is made at 11 K. The addition of the 26DNT impurity causes several of the 24DNT resonances to disappear (indicated by the blue arrows).

Figure 9 shows the effect of the doping for each case on the cryogenic waveguide THz-TDS spectrum. For the case of the doped AN film the KN impurity introduced at 3% by weight induces a noticeable line broadening of the AN vibrational resonances as well as some change in the relative intensities of the resonances [16]. The line broadening is attributed to an increase in disorder in the AN lattice. In contrast, the effect of the 26DNT impurity on the THz spectrum of 24DNT is more dramatic. Here, the 26DNT impurity at 6% by weight causes six of the vibrational resonances of 24DNT to disappear. This suggests that the 26DNT impurity diminishes the long-range vibrational coherence in the lattice and therefore reduces the intensity of many of the phonon modes. These experiments represent an initial step towards understanding how impurities affect THz of molecular solids. More work is needed to fully understand the mechanism by which the impurity alters the THz spectrum. This type of understanding is considered by us to be essential for potential implementations of THz spectroscopy to the identification of unknown materials found in the field.

Summary and Outlook: The significantly narrow vibrational resonances that have been demonstrated with waveguide THz-TDS together with the high sensitivity of the sub-wavelength PPWG gap suggest that there is some potential to use the method for materials identification. It's important to note, however, that the high resolution occurs at cryogenic temperature, therefore using waveguide THz-TDS for on-the-fly analysis in the field would seem impractical. Instead we envisage potential applications where unknown materials found in the field are returned to a site where analysis is carried out. Even so, there remain issues that must be addressed. One issue is the need to improve the practicality of the PPWG by simplifying the coupling of the THz field. The current implementation uses Si lenses for coupling of the THz field, which requires a rather time-consuming alignment procedure. An alternative is to use tapered metal surfaces that can collect the free space THz radiation and guide it into the sub-wavelength gap like a funnel, such as shown in the diagram below. This principle relies on the fact that THz waves can be regarded as microwaves to some extent. Recently, machine tapers and metal flare couplers have been shown to simplify the coupling of THz waves into the gap and have even shown promise for high resolution spectroscopy of polycrystalline molecular films [17].

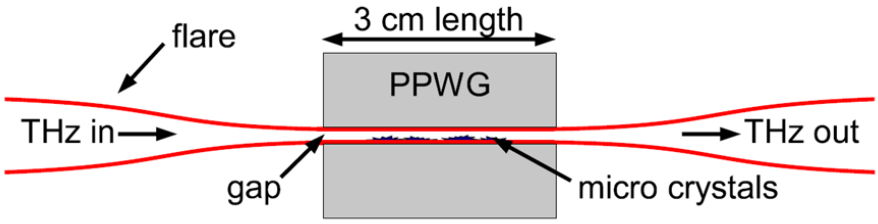

A more fundamental issue involves gaining a better understanding of how impurities and defects affect the THz spectrum. Our initial results suggest that impurities can lead to moderate broadening of the vibrational resonances due to increased sample disorder, or in some cases the impurity can lead to a more dramatic change in the THz spectrum of the parent material where some vibrational resonances of the parent material disappear. At first glance dramatic alterations of the THz spectrum caused by impurities seem to compromise applications. However, if certain impurities or additive can be shown to cause specific and reproducible changes, then there may unique value to THz spectroscopy for forensic type identification. Clearly there is a need for more fundamental work to understand how impurities, defects, and sample aging affect the THz vibrational spectrum.

From a more fundamental point of view, a wider range of different samples have to be investigated to understand the generality of using waveguide THz-TDS. In particular, additional knowledge about complex samples needs to be built up, leading to deeper understanding in fields of biology and chemistry. For example, it will be important to build up from the rather medium-sized molecules investigated in this project to larger more complex molecules, where it would be interesting to investigate the limit where the density of states begins to blur the narrow resonance structure, even at cryogenic temperatures.

2. Long Path THz Pulse Propagation and Detection of Vapors in the Ambient Atmosphere

Introduction: The remote sensing of molecular gases and vapors in the region between 0.1 – 1.0 THz is a challenging problem, in part because of strong absorption of THz radiation by atmospheric water vapor. Even so, there are windows of relatively high transmission, especially at the lower THz frequencies, where transmission over paths greater than 100 meters is feasible [18]. One goal of this part of the program is to create methods to propagate ultrashort broad bandwidth THz pulses in the ambient laboratory over pathlengths longer than 100 meters and characterize the effect of the ambient atmosphere on the pulse propagation. A second major goal is to assess the ability of the ultrashort THz pulses to detect the rotational signatures of target vapors when propagating over long paths (> 100 meters) in the presence of interference from water vapor.

For active detection of analyte vapors at ground level there have been a few examples where narrowband cw techniques have been applied to the detection of gases. For example millimeter radar chemical sensors have been constructed based on a continuous-wave narrowband backward wave oscillator (BWO) source using the transparency window from 0.22 – 0.30 THz [19]. In contrast, there have been only a few studies of broadband coherent THz pulse propagation in the atmosphere [20], and to our knowledge there have not been studies to characterize the ability of broadband THz to detect target gases and vapors in the ambient environment. An important motivation for using a coherent broadband THz-TDS system is the potential to transmit significant spectral amplitude over relatively long paths in each of the atmospheric transparency windows. For small molecule gases and vapors that have sufficiently resolved rotational structure at atmospheric pressure, broadband detection provides an opportunity to simultaneously detect a relatively large number of rotational lines (or bands) in the transparency windows, which can increase the robustness of identification. As an example to illustrate the potential the rotation spectrum of methanol vapor is simulated at low pressure and at atmospheric pressure in Fig. 10. At low pressure the individual rotational transitions are largely resolvable and the rotational spectrum provides a highly precise fingerprint for identification. At ambient pressure the pressure broadening effect broadens the individual transitions (approximately 5 GHz FWHM) such that they merge into band spectra. Even so, several of the bands occur within atmospheric transmission windows, so that if broadband detection is possible then the detection of multiple bands simultaneously can lead to more robust identification.

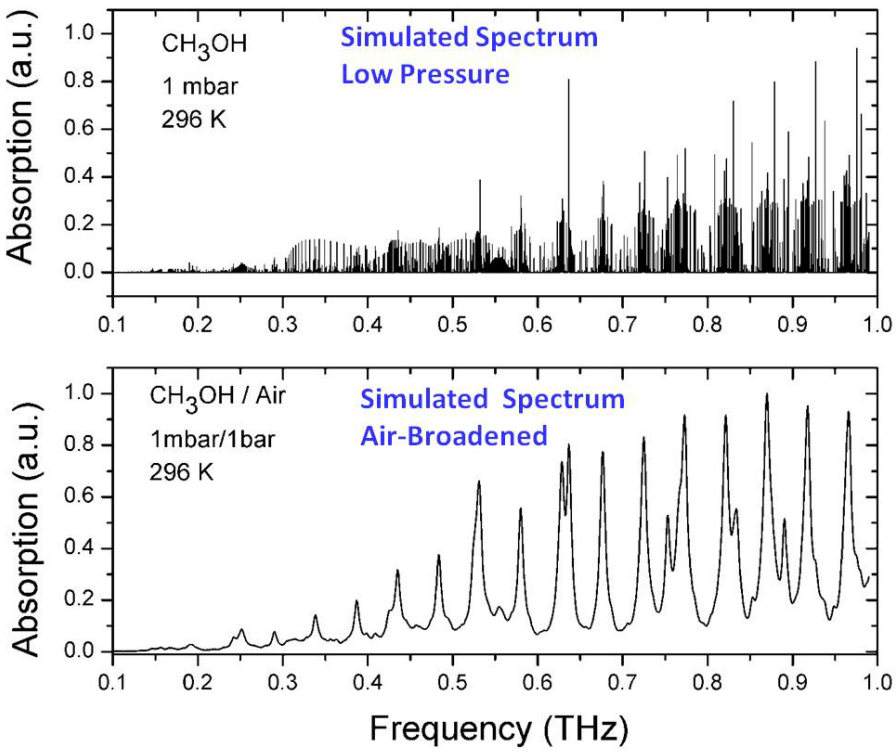

Fig. 10. Simulated rotational spectra of methanol vapor under low pressure conditions (1 mbar) and at ambient pressure (1 bar).

Experimental Methods: The apparatus used for propagating ultrashort THz pulses in the ambient laboratory environment is based on a standard THz time-domain spectrometer (THz-TDS) [8] that is modified with deflecting mirrors to send out and return a low power (10-30 nanoWatts) THz beam.
Two experimental apparatus were used for pulse propagation studies and subsequent measurements of analyte vapors contained within a path external to a conventional THz spectrometer. The first apparatus transmits the THz beam over a relatively short roundtrip path length of 6.7 meters. The beam path includes propagation in a long tube chamber where analyte vapors can be introduced. This apparatus will be referred to as the "long-tube" apparatus [21]. Using the THz pulse propagation experience gained from the long tube apparatus we then constructed a second apparatus which transmits the THz beam over a much longer open path of 170 meters and is called a "long-path" apparatus [22,23]. Both of these apparatus are based on a modified optoelectronic THz-TDS spectrometer. We briefly describe these apparatus below with some modifications for the detection of vapors.

A schematic of the long-tube apparatus is shown in Fig. 11. The THz spectrometer is contained in dry-air purged box #1. The THz beam is coupled out of the spectrometer by a removable mirror pair and into dry-air purged box #2 through a 15 cm diameter thin (12.5 μm) film plastic window, which is highly transparent and has very little reflection. Box #2 is connected to a 6" (15.24 cm) inner diameter commercial PVC pipe. Both ends of the pipe are sealed with thin film plastic windows so that it encloses an air-tight round trip path length of 5.4 meters.
The THz beam is returned through the tube and to the receiver using a 6" (15.24 cm) diameter concave spherical mirror with a 120" (3.04 m) radius of curvature. The total extra round trip

distance of the path external to the standard spectrometer path is 6.7 meters. This distance is equal to 2 round trips of the ultrafast pulses in the titanium sapphire pump laser cavity with a repetition rate of 89.695 MHz. Therefore, to gate the receiver we use the second pulse down the pulse train from the optical pulse that gates the transmitter (see Fig. 11). A picture of the long tube apparatus setup at Oklahoma State University is also shown in Fig. 11. The entire apparatus in contained on a single optical table.

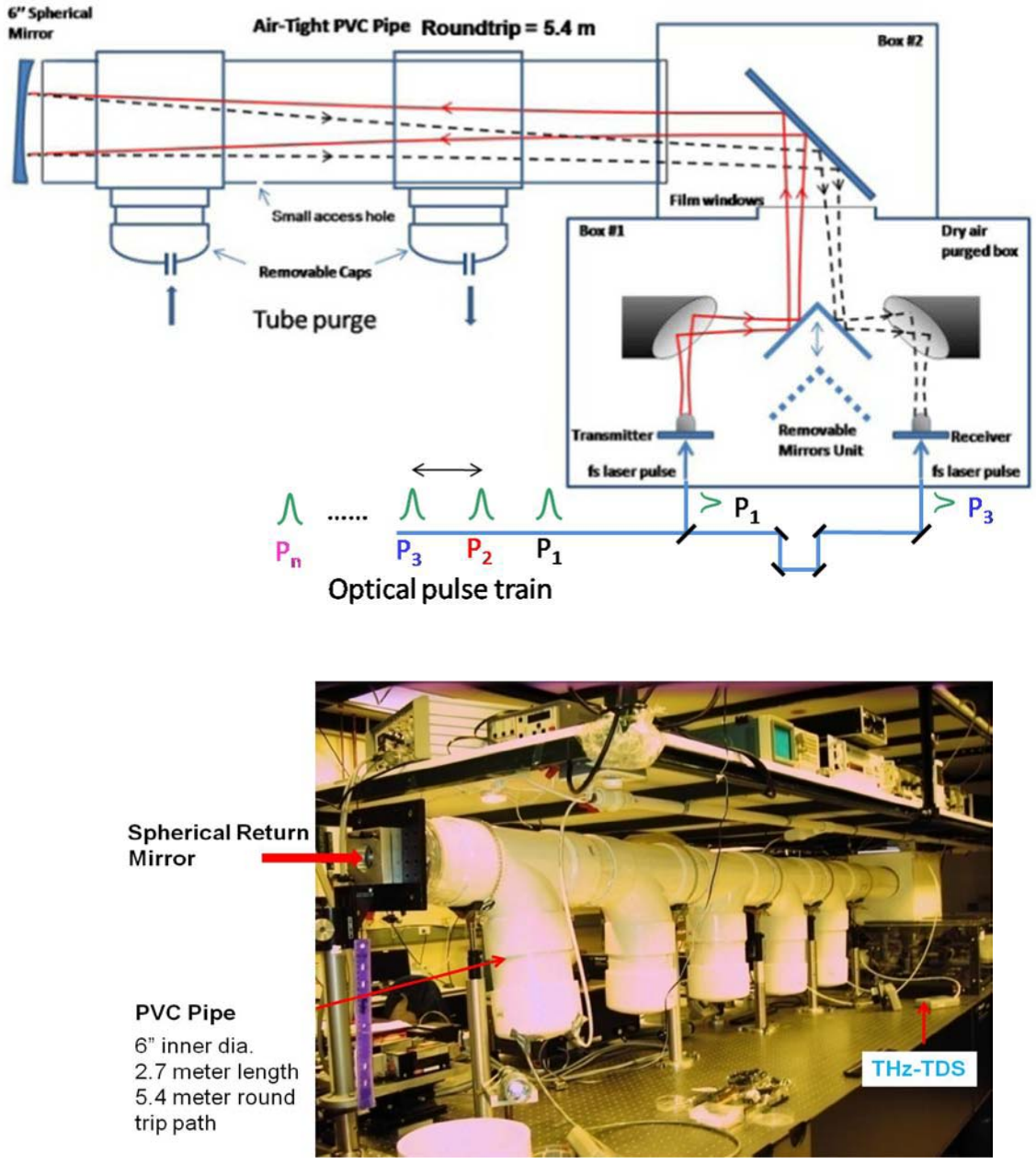

Fig.11.Top: Schematic of long-tube apparatus based on a standard THz-TDS spectrometer. A pair of removable mirrors deflects the THz beam out of the spectrometer and into Box #2. The beam then enters a 5.4 meter round trip path length enclosed tube for vapor measurements. The THz pulse returned to the receiver is gated by the 2nd pulse (P3) down train from the pulse that excites

the transmitter (P1). Bottom: Photograph of the long tube apparatus showing the 2.7 meter PVC pipe used for environmental control and introducing target vapors.

A schematic of the long-path apparatus is shown below in Fig. 12. Photographs of the optical apparatus at Oklahoma State University are shown in Fig. 13. The apparatus uses the same THz-TDS spectrometer but differs from the long-tube apparatus in several ways. First, the entire apparatus (with the exception of the sample tube) including the spectrometer is in the ambient environment. Second, to reduce diffraction losses relatively large mirrors (Edmund Optics) are used to guide the THz beam. The collimating mirror M3 has a diameter of 12.5" (32 cm) and a 125" (317.5 cm) focal length. M4 = 16" x 24", M5 = 12" x 12", and M6-M10 = 16" x 24". Third, the sample tube consists of a 12" (30.5 cm) diameter 24" (61 cm) long clear Plexiglas tube fitted with air-tight thin film plastic windows on both ends. For convenience the sample tube is placed on the optical table between mirrors M2 and M3 (In principle, placement anywhere along the path would effectively result in the same double pass). The total round trip sample path length is 1.2 meters, which is 4.5 times shorter than the long tube described above.

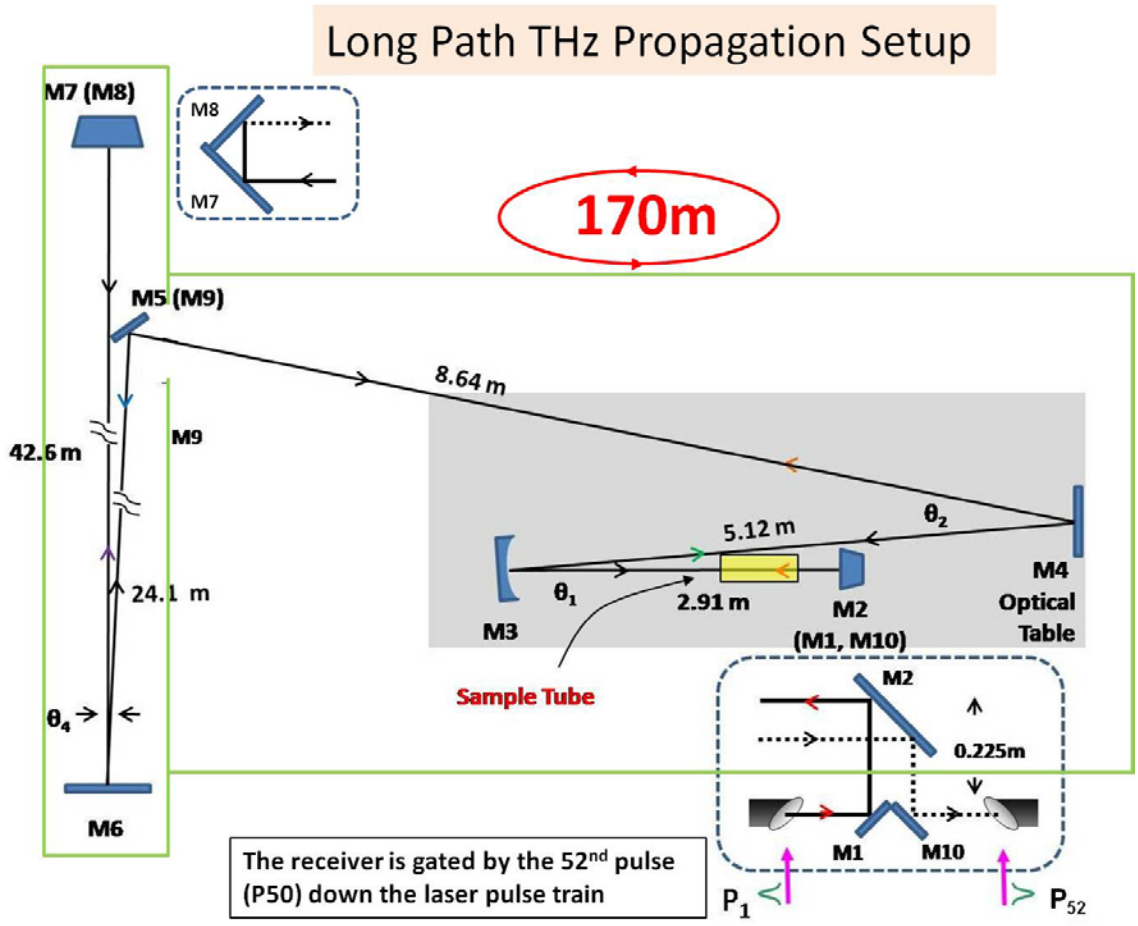

Fig. 12. Schematic from the top (x-z plane) of the 170 meter round trip long path apparatus consisting of 10 mirrors. Insets: Side view (y-z plane) of the mirrors. The solid lines show the path of the THz beam deflected out of and into the spectrometer by the mirror pair M1 and M10. The position of the THz-TDS spectrometer is shown in the inset and lies underneath M2.

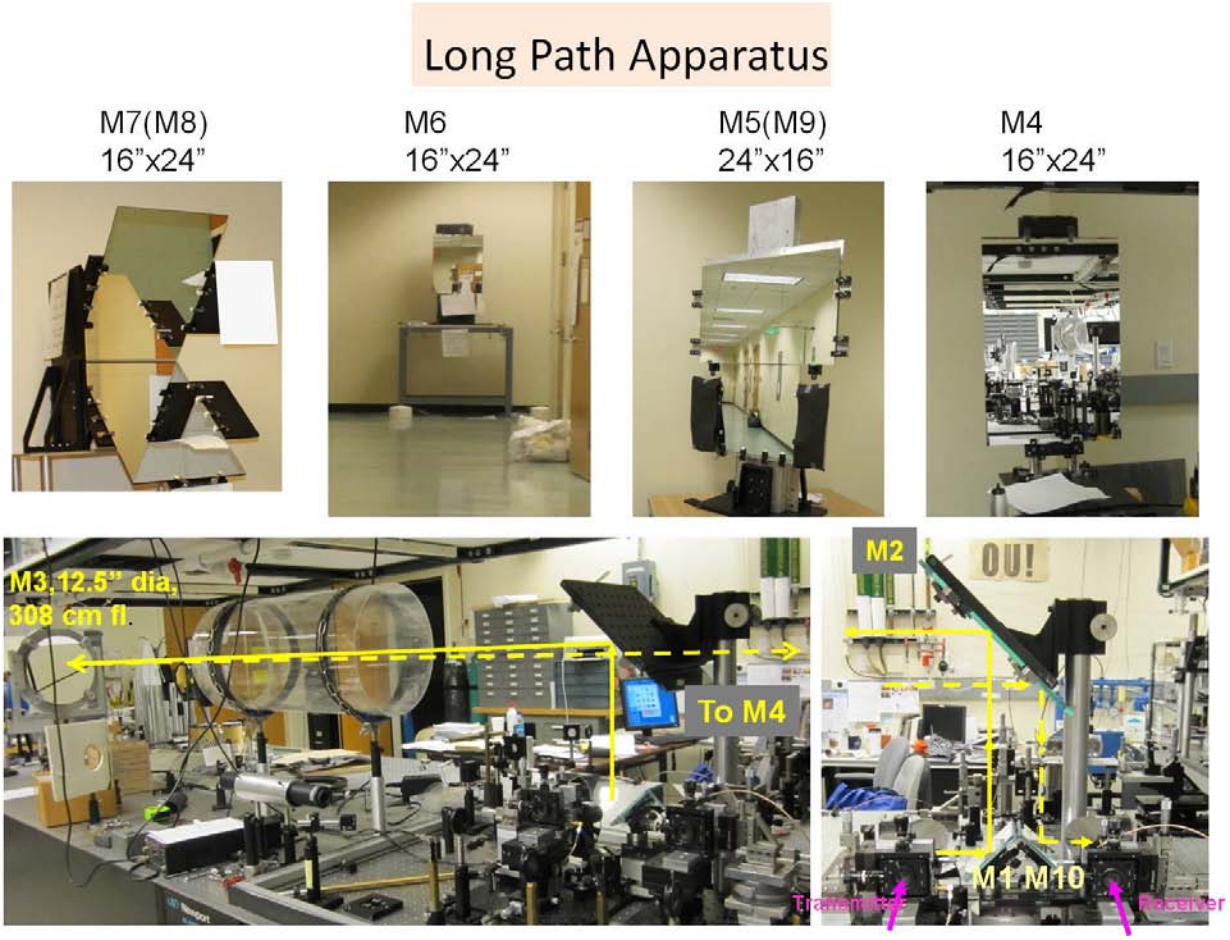

Fig. 13. Optical apparatus of the 170 meter round trip long path apparatus at Oklahoma State University. Mirrors M1-M4 and M10 are contained in the THz laboratory. Mirrors M5-M9 are contained in the adjacent hallway.

The alignment of the THz beam is quite stable considering that it first propagates along an optical table via M1-M4, and then propagates through the rest of the laboratory using floor mounted mirrors (M5-M9). There is a slow thermal drift in the pulse train of about 0.6 ps/hr, corresponding to a drift of 180 μm/hr, which is about 1 part-per-million of the 170 meter path. The thermal drift is quite slow compared to the three minute measurement time to scan a waveform. The repetition rate of the mode-locked laser without any special features is quite stable at 89.6948(x)(x) MHz with frequency drift and some jitter in the last 2 digits indicated by x in the open brackets. The above repetition frequency corresponds to a delay between pulses of 11.148918 ns, which is multiplied by 51 to give the total laser-clock defined long-path delay of 568.594835 ns. Over the course of an experiment, there are slow changes of the order of 100 Hz. If the clock rate is reduced to 89.6947 MHz, the corresponding total time delay is increased to 568.595469 ns, causing a difference in the total long-path clock delay of 0.63 ps. This change in delay is easily measured and is almost equal to our observed drift of 0.6 ps/hour.

Results:

Long-Tube Measurements: The THz pulse propagation and measurement of the absorption due to atmospheric water vapor was determined as follows. First, the system operation and stability

are checked by measuring performance of the THz-TDS system in box #1 with the coupling mirrors removed. Second, the coupling mirrors are re-installed in box #1, which is then refilled with dry air, as well as box #2 and the PVC pipe system. Then, the THz reference pulses, transmitted through the entire system filled with dry air, are measured. Third, the THz sample pulses, transmitted through the PVC pipe system with the cap removed and box #2 open to laboratory humid air and with box #1 filled with dry air, are measured. Then, again the reference pulses are measured. This sequence is repeated several times during the complete transmission measurement. Fig. 14 compares the input THz pulse and spectrum to the THz pulse and spectrum after propagating through the long tube at 51% relative humidity (RH). The reference and sample pulses are measured over one scan duration of 165 ps, corresponding to the frequency resolution of 6.1 GHz. A scan consists of 625 channels (data points) with 40 μm steps between channels, corresponding to the double pass (80 μm) time step of 0.2667 ps between channels. A single scan takes 180 seconds. For a complete experimental measurement series, 4 reference dry-air pulses and 4 sample humid-air pulses were measured.

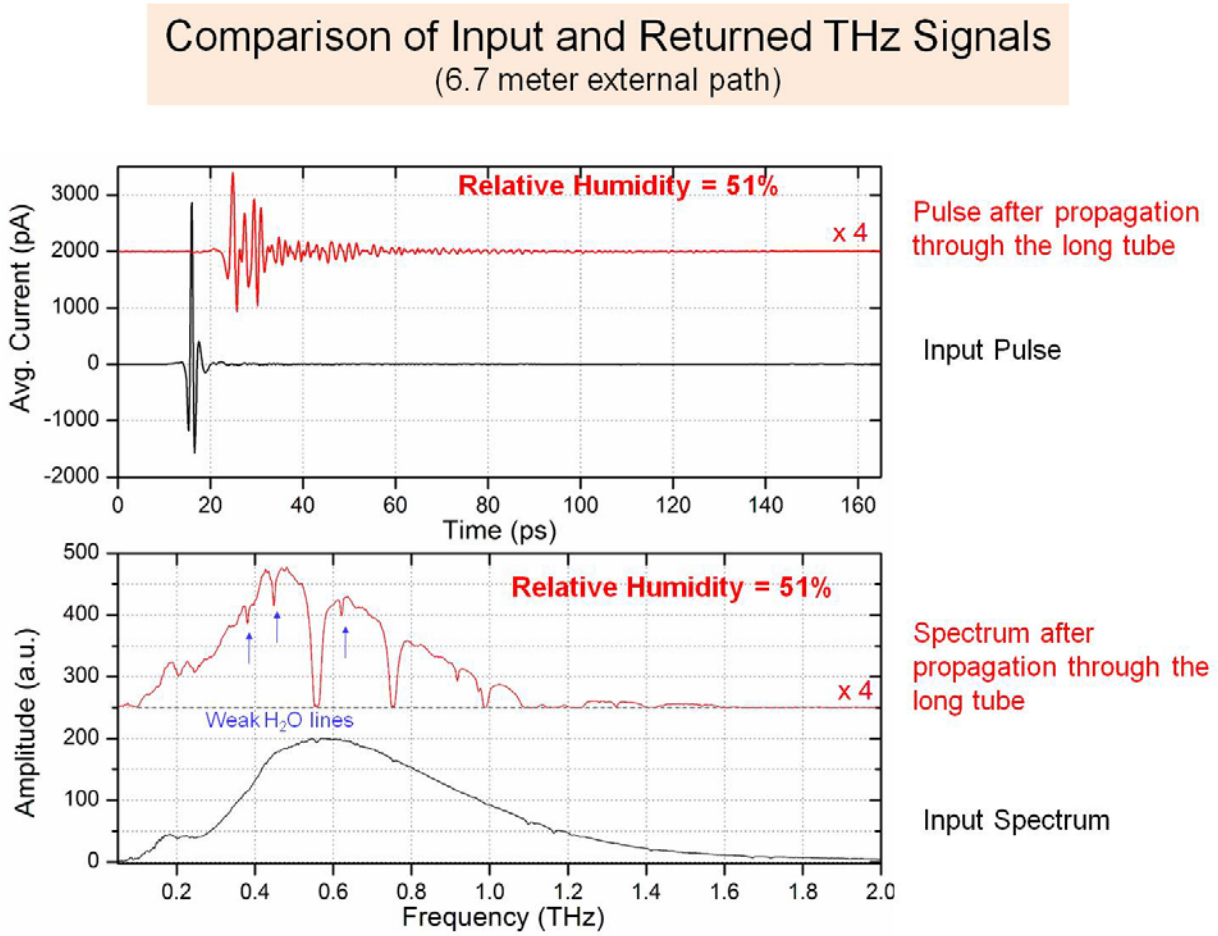

Fig. 14. Input and returned THz pulse and spectrum in the long tube apparatus.

The input THz pulse (electric field) is essentially a single cycle pulse with a sub-picosecond pulsewidth (FWHM) and has a smooth spectrum that extends from below 200 GHz to approximately 2.0 THz. The THz pulse returned after propagating 6.7 meters through two boxes

and PVC tube has been strongly modulated by the interaction with water vapor at 51% RH. The ringing signal on the THz pulse extends to the full 165 ps time window and is due to the absorption by the rotational transitions of H_2O vapor that overlap the pulse bandwidth. The amplitude spectrum shows essentially complete absorption from the strong H_2O transitions and the significant appearance of the very weak water lines at their handbook frequencies and with resolution limited linewidths.

The amplitude spectral coupling from the mirror in box #1 to the 45 degree mirror in box #2 and into and through the tube to the 6 inch end mirror and then retracing the same path, but with a slight tilt to return the beam to box #1 and onto the mirror directing the beam to the THz receiver, reduces the amplitude spectrum of the reference pulse by the factor 0.35 with the corresponding factor of 0.33 for the pulse amplitude. This good coupling preserves our excellent signal to noise ratio (S/N); for the THz signal pulse, S/N = 700, while for the corresponding amplitude signal spectrum S/N = 200 [21].

The high resolution broadband THz-TDS long tube apparatus described above was used to measure the power attenuation of the transmission windows from 0.2 THz to 1.0 THz and the power attenuation of the weak water vapor lines within the same spectral range. Our measurements were compared to theoretical models of atmospheric attenuation. Our experimental results were found to agree better with models that include the attenuation of the atmospheric moist air continuum (or extra water vapor absorption) [21].

The long tube apparatus was then used to assess the ability to use THz-TDS to detect target vapors contained in the long tube in the presence of interference from H_2O vapor. The example discussed here is for acetonitrile (CH_3CN) vapor. Other vapors including D_2O [23], CH_2Cl_2 and HCl were also measured. The CH_3CN vapor was introduced in the PVC tube by placing known volume of liquid into tube and allowing the vapor to fully equilibrate.

The time domain response of CH_3CN vapor is shown in Fig. 15, which is contained in the long tube at a concentration of 200 parts per million (ppm), and in the presence of low RH of 14%. CH3CN is a symmetric top molecule and its rotational spectroscopy has been well studied using high resolution methods. For the case of atmospheric pressure broadening the rotational constant B is approximated as 9.199 GHz [24], which leads to a manifold of equally spaced rotational transitions separated by twice the rotational constant, 18.40 GHz. This separation is sufficient to allow resolution of the $J \rightarrow J + 1$ rotational bands under ambient pressure.

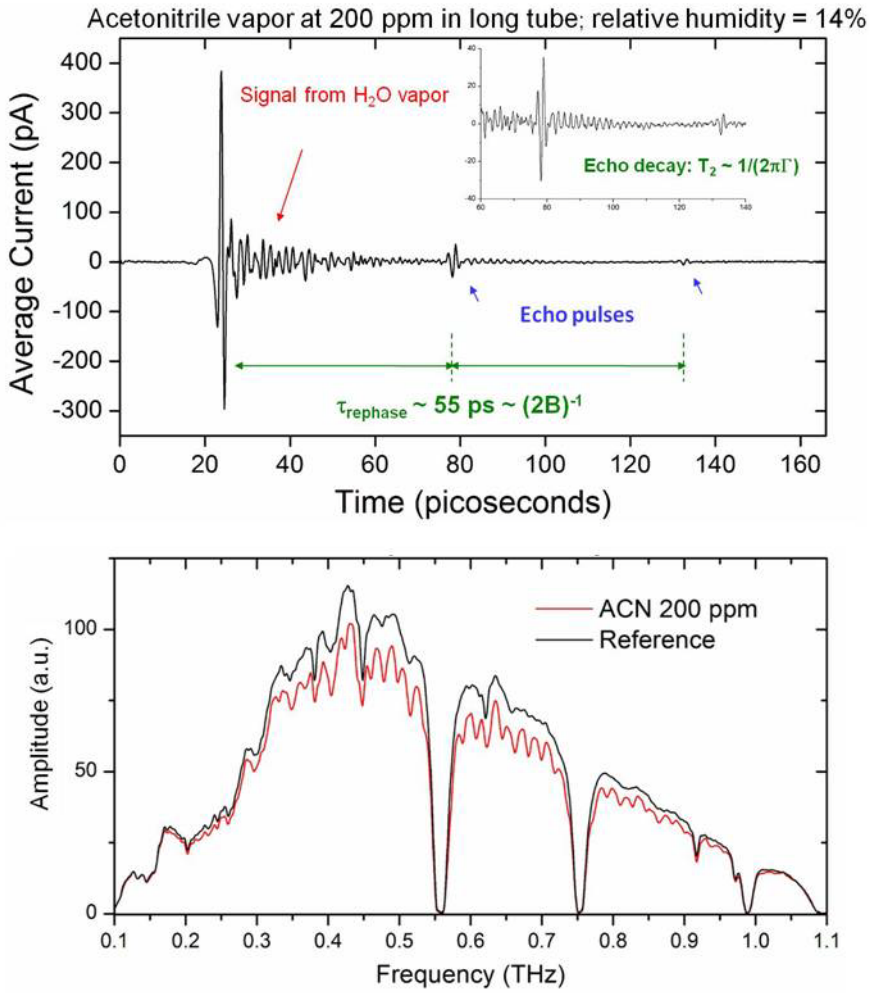

Fig. 15. Signal waveform (top) and spectral amplitude (bottom) for CH3CN contained in the long-tube chamber at a concentration of approximately 200 ppm. The RH in the chamber was 14%. The inset shows the time base expanded in the echo region. The saturated absorption dips in the spectral amplitude are due to the strong water vapor rotational transitions.

Figure 15 (top) shows the signal waveform (average of four measurements) where the long tube sample chamber contains CH3CN at a concentration of 200 parts per million (ppm). The RH in the sample tube was 14%. The waveform contains two components. The highly oscillatory pattern with large amplitude at early times is due to the interaction with the rotational transitions of water vapor. This signal decays sufficiently to expose a second component which consists of echo-like pulses centered near 79 ps and 133 ps. The echo pulses are a consequence of the coherent excitation of (nearly) equally spaced rotational transitions of the symmetric top molecule. Figure 15 (bottom) shows the Fourier transform of the waveform. Here, the spectral amplitude clearly shows the equally spaced rotational absorption bands. Superimposed on the spectrum is the nearly complete absorption due to the strong water vapor transitions at 0.55 THz, 0.75 THz, and 0.98 THz.

The experimental spectrum for CH_3CN was compared to the theoretically predicted spectrum using database values for the CH_3CN line frequencies and line intensities, which are tabulated in the JPL spectral line catalog [25]. In the computation we used rotational values for the ground vibrational state of CH_3CN and rotational values the low frequency excited vibrational level (v8)

at 365.05 cm^{-1}. At room temperature the THz absorption from vibrationally excited CH_3CN is non-negligible (v8 for CH_3CN is doubly degenerate, however the JPL database only provides rotational values for v8=1). Our calculated peak amplitude absorbance of about 0.31 is in approximate agreement with the peak experimental absorbance of 0.25. We note, however, that the calculated absorbance does not contain contributions from CH_3CN (v8 = 2). A comparison of the peak band frequencies of experimental and calculated spectra showed excellent agreement to within 1 GHz.

Long Path Measurements: Figure 16 shows the effect of the external 170 meter path propagation on the THz pulse and spectrum in the ambient laboratory environment at 50% RH. Here, the interaction with the water vapor rotational transitions has dramatically broadened the oscillatory pattern so that the oscillatory signatures are still visible at 160 ps. The broadening of the oscillatory pattern has been attributed in part to group velocity dispersion resulting in a frequency swept waveform, with the higher frequency components trailing the lower frequency components [22]. The peak amplitude has been further reduced by the increased water vapor absorption and losses due to the frequency dependent amplitude coupling which includes diffraction losses. The frequency dependent amplitude coupling is described in quantitative detail in reference [22].

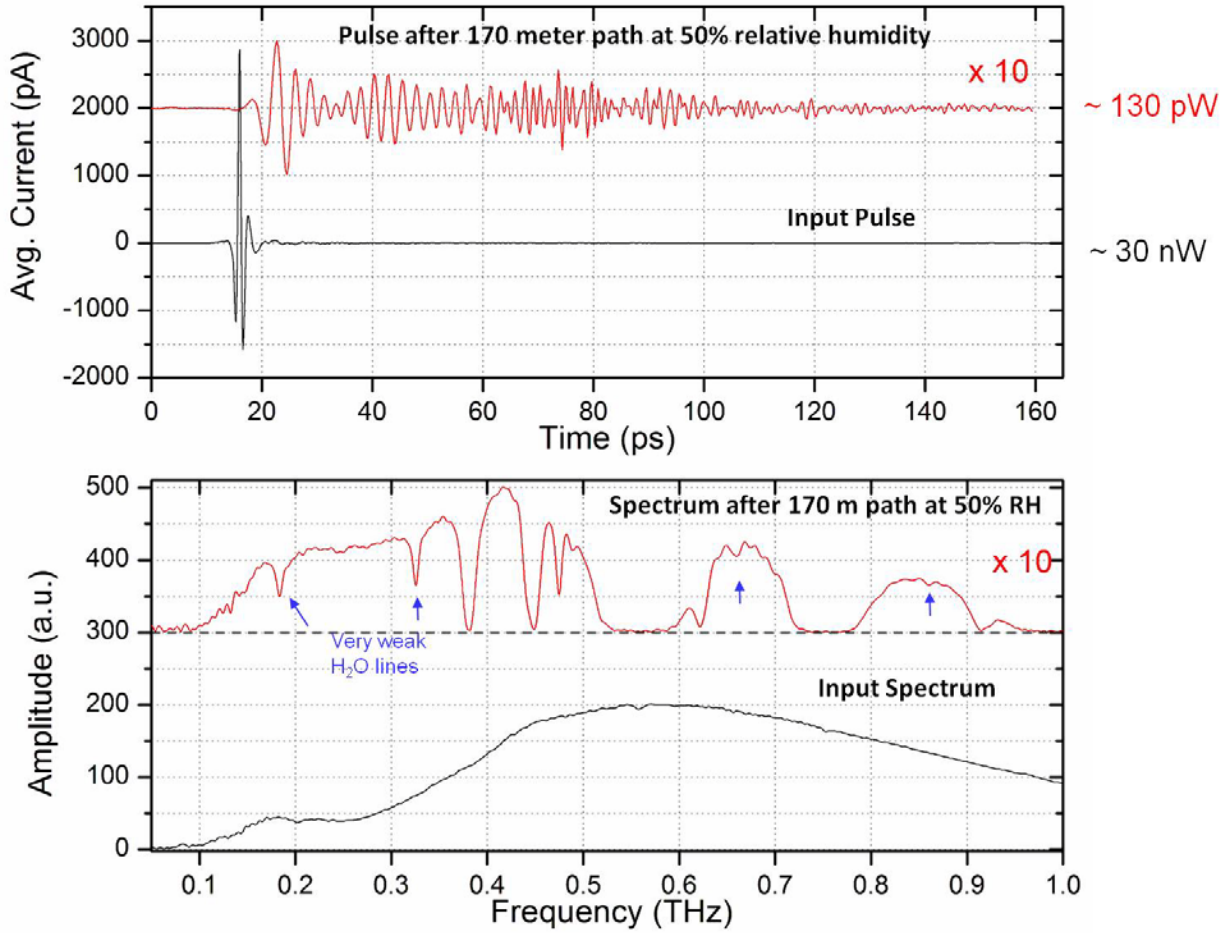

Fig. 16. Effect of atmospheric attenuation on the 170 meter THz pulse propagation in the ambient environment at 50% relative humidity. Top: Experimental waveforms for input and returned THz waveforms. Bottom: Input and returned amplitude spectra.

The waveform and spectral amplitude curves are the average of six measurements. With this level of averaging the peak S/N for the waveform is approximately 200:1. The average transmitted power was 130 pW. The 170 meter path propagation at 50% RH limits the transmission of frequency components to a maximum of about 0.95 THz. In addition, very weak water vapor transitions now appear in the spectrum at 0.184 THz, 0.326 THz, 0.474 THz, 0.659 THz, and 0.861 THz. Despite the strong effect of water vapor absorption there remain several regions of relative transparency which can be used for vapor sensing.

The measurement of target vapors over the much longer 170 meter round trip path is more challenging because of increased water vapor absorption, greater fluctuations in humidity, and thermal and mechanical fluctuation we demonstrate the ability of the long-path apparatus to measure the rotational spectra of CH_3CN and a HDO/D_2O mixture. Figure 17 shows the absorbance spectrum of CH_3CN vapor at 800 ppm in the sample chamber. The relatively high vapor concentration was used because of the short 1.2 meter round trip path sample tube. In the measurement, six reference waveform scans were collected first (no CH_3CN in the chamber) and the spectral amplitudes averaged to obtain the reference spectrum. CH_3CH was then introduced to the chamber and allowed to equilibrate, and six signal waveforms collected and the spectral amplitudes averaged to obtain the signal spectrum. As a check of the system and environmental stability, a second set of six reference scans were taken. Typically we found that the two sets of reference spectra showed agreement to within 5%. A full sequence of measurements required about 1 hour to complete.

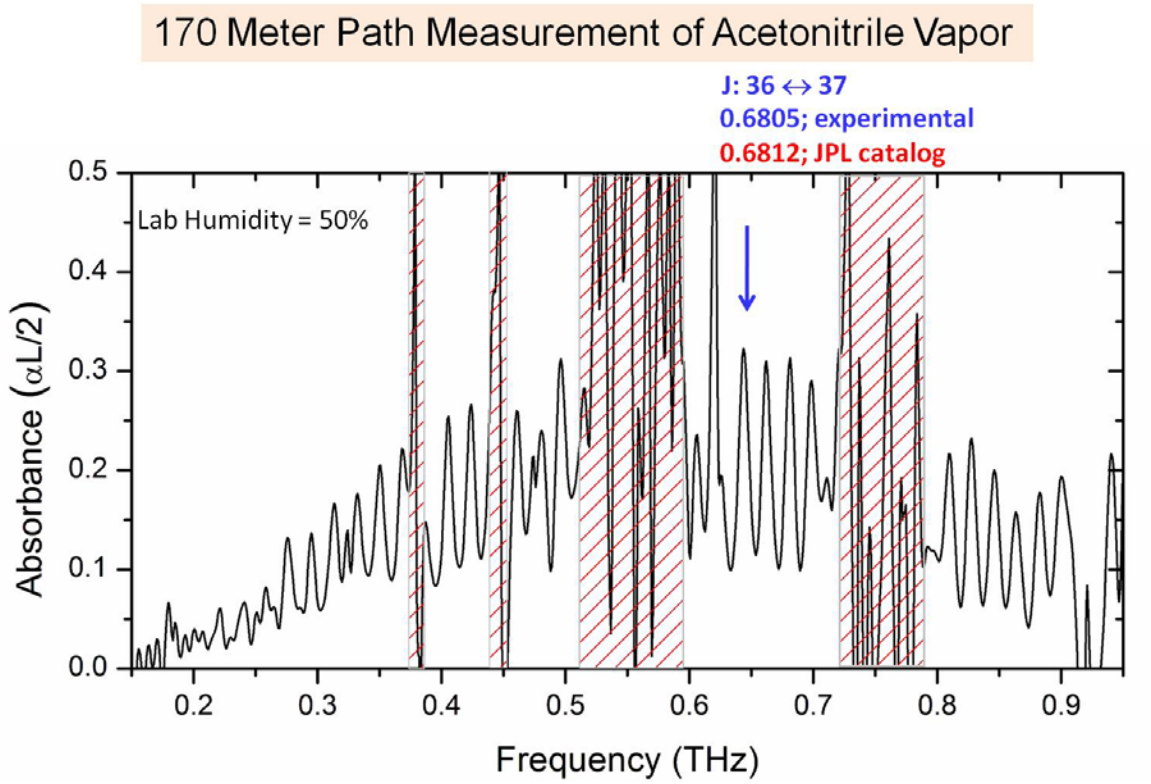

Fig. 17. Amplitude absorbance spectrum for CH3CN vapor at 800 ppm in the 1.2 m (round-trip) sample chamber measured using the 170 meter long-path apparatus. The laboratory relative humidity was 50%. The hatched areas indicate regions of complete water vapor absorption.

The hatched areas in Fig. 17 indicate regions of complete absorption by water vapor, consequently rotational transitions of the analyte cannot be observed in these regions. However, in the transmission windows as many as 20 rotational bands can be observed. A measure of the minimum detectable absorption is given in Fig. 18 showing the noise baseline recovered from averaging six pairs of reference measurements. Depending on the position within the transmission windows the minimum detectable amplitude absorption (S/N ~1) varies between 2.5 – 5%.

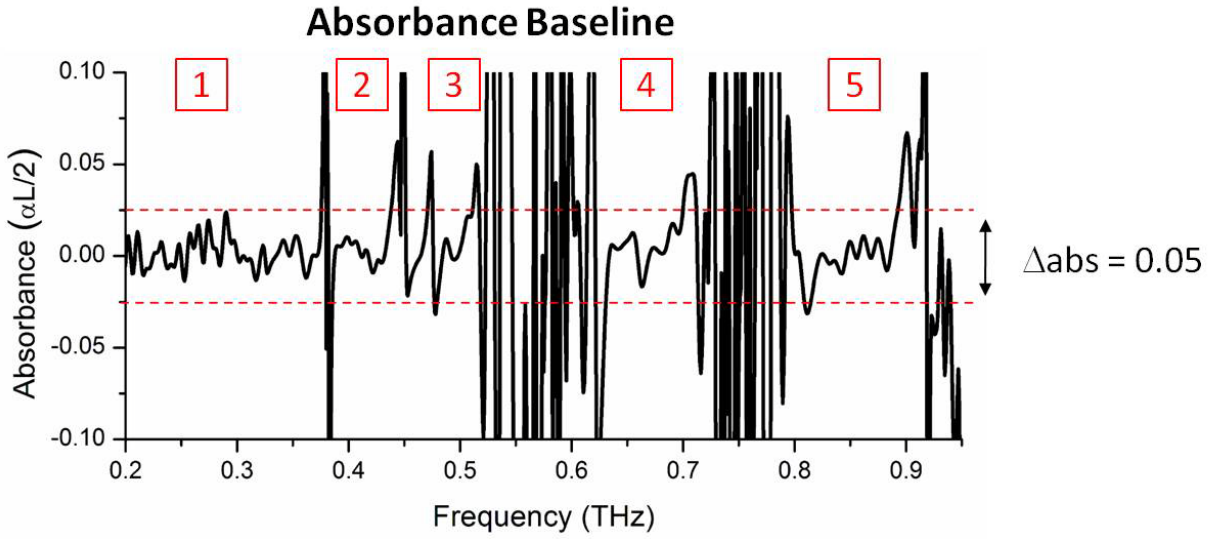

Fig. 18. Detection sensitivity for the 170 meter path apparatus resulting from the averaging of six pairs of reference measurements. The red horizontal bars provide a qualitative measure of the noise level in the amplitude absorbance. The square boxes indicate the widows of relatively high THz transmission.

The second example shown below in Fig. 19 is the detection of a HDO/D2O vapor mixture contained in the sample chamber within the 170 meter THz path. Here, D2O liquid is initially evaporated in the sample chamber in an amount equivalent to a vapor concentration of approximately 3000 ppm. Despite the strong effect of water vapor absorption seven absorption lines marked by blue arrows can be distinguished from the noise floor and are due to the analyte vapors. The red curve is the fit to the experimental spectrum based on a superposition of HDO and D2O database line frequencies and relative line intensities. The best fit occurs for a 2.4:1 ratio of HDO:D2O. Compared to the long-tube case, a smaller percentage of the initial D2O introduced to the chamber has converted to HDO. Also from the fit we find that the accuracy of the experimental line frequencies is within 1.5 GHz of the JPL catalog values. This finding is an indication the stability of the long-path apparatus over the approximate 1 hour time to perform the reference measurements, introduce and equilibrate the sample, and the perform the signal measurements.

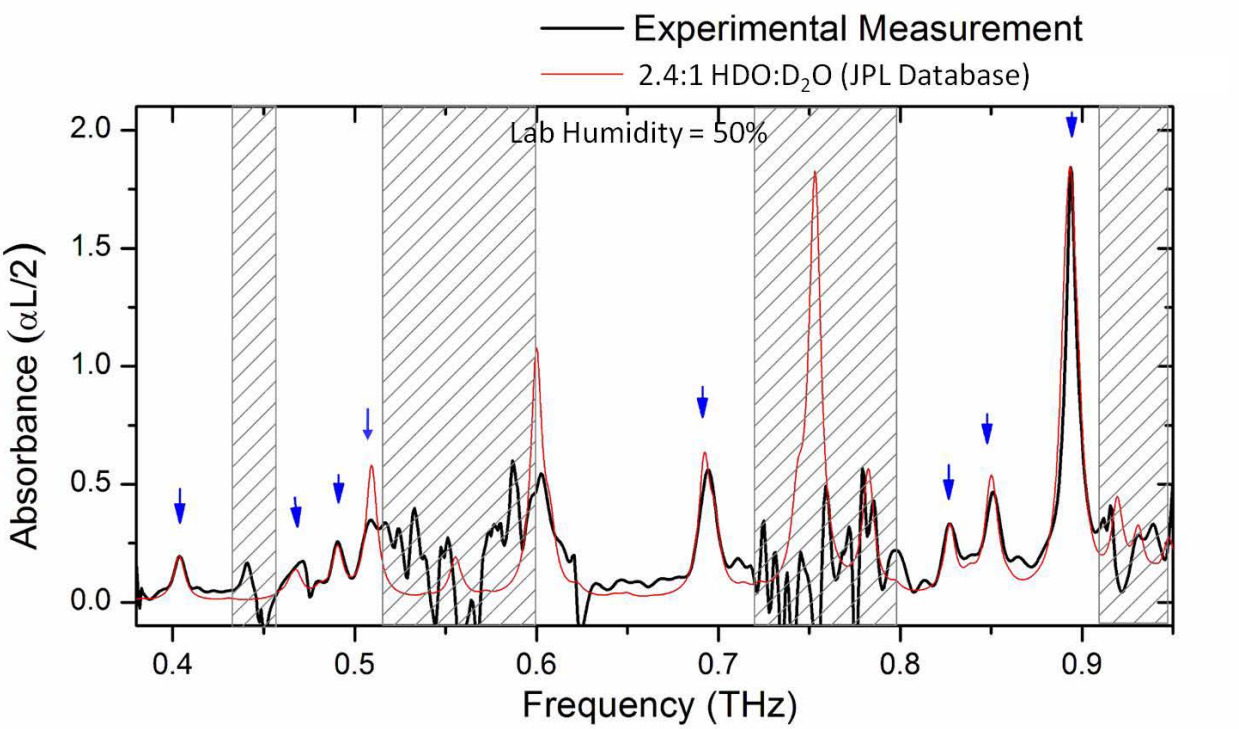

Fig. 19. Experimental amplitude absorbance spectrum (black curve) where D2O liquid is introduced into the 1.2 m (round-trip) sample chamber to give a concentration of approximately 3000 ppm. The relative humidity in the laboratory and sample chamber is 50%. The hatched areas indicate regions of complete absorption by water vapor. The red curve is a fit to the experimental spectrum using rotational line frequencies and line intensities for HDO and D2O contained in the JPL catalog.

It's useful to scale the extrapolate the experimental results above to sample pathlengths that might represent a realistic plume. This is done in Fig. 20, which considers the current experimental configuration capable of detecting a minimum amplitude absorbance of 5% with S/N = 1. The rotational frequencies are chosen to fall within an atmospheric transmission window. The round trip path is taken to be 100 meters to simulate a plume. Under these conditions the concentrations needed for detection of a rotational band for CH_3CN at 0.691 THz and the rotational line of HDO at 0.893 THz are 1.3 ppm and 4.5 ppm, respectively. The detection of CH_3CN and HDO may be compared to projections for relatively strong (HCN) and relatively weak (NO_2) THz absorbers.

	Vapor	Frequency	Current Sensitivity 5% Absorption; S/N ~1
	CH_3CN	0.681 THz	1.3 ppm
	HDO	0.893 THz	4.5 ppm
Strong →	HCN	0.895 THz	130 ppb
Weak →	NO_2	0.840 THz	220 ppm

Fig. 20. Projection for minimum detectable concentrations when scaled to a 100 meter round trip sample path in current THz-TDS long path apparatus

Summary and Outlook for Detection of Vapors: Using a modified THz-TDS spectrometer we have demonstrated detection of rotational spectra of analyte vapors located remotely from the spectrometer and under ambient laboratory conditions of temperature, pressure, and humidity. Two types of apparatus were investigated. First, in the long-tube configuration the detection of the signature echo pulses from CH3CN was demonstrated in the presence of low relative humidity of 14%. The interference of the water vapor signatures obscures the echo transient at the higher relative humidity of 51%. However, here, we were able to detect the absorbance spectra of analyte vapors over a broad range of frequencies from 0.2 - 1.6 THz. The minimum detectable amplitude absorption was shown to be approximately 1%. Second, we demonstrated detection of rotational transitions when the THz beam propagated over a much longer 170 meter open path in the ambient laboratory environment, subject to increased losses due to water vapor absorption, amplitude coupling and diffraction, as well as increased environmental fluctuation in humidity, temperature, and mechanical vibration. In this more challenging environment we showed that the long-path apparatus had sufficient stability to detect rotational line amplitude absorption as small as about 3-5%. The increased THz loss due to water vapor absorption limited detection to the transparency windows below about 1 THz. To our knowledge, both of these demonstrations represent the first of their kind for broadband ultrashort THz pulses.

To assess the potential of using broadband THz pulses for remote sensing applications it's important to discuss current limitations in detection sensitivity, as well as the type of vapors where this method can achieve specificity. Our current THz-TDS system uses only about 10 mW of optical power to gate each the transmitter and receiver, out of more than 300 mW that is available. The 10 mW optical beam generates a low power beam of THz pulses with about 30 nW of average power. After propagation of 170 meters, with losses due to water vapor absorption, coupling back to the receiver, and diffraction, it was determined in Ref [18]. that the returned power was reduced to 130 pW. Even so, the THz waveform can be measured with S/N of 200 (baseline to peak). There is potential to significantly increase S/N through a combination of increasing the generated THz power, optimizing the THz pulse spectrum for overlap with the atmospheric transparency windows, and reducing diffraction loss. For example, by using larger feature size photoconductive antennas, or interdigitated antennas [28], it should be possible to gate the transmitter and receiver with 100 mW of optical power. In principle, this modification alone could lead to a 100-fold increase in the detected THz signal power. Higher THz power levels would be useful to reduce the signal acquisition time for detection.

Pressure broadening places a limitation on the generality of THz sensing of vapors in the ambient environment. The relatively light molecules discussed here represent favorable cases because of the small partition functions and large separation between rotational lines. Qualitatively, for molecules that can be described as symmetric tops, a 5 GHz FWHM pressure-broadened line width implies that the rotational constant (total angular momentum) should not be much smaller than 5 GHz in order to at least partially resolve the rotational bands. Therefore, at atmospheric pressure, specificity is maintained only for the class of relatively small and light vapor molecules with relatively large rotational constants. However, it should be mentioned that the detection of small molecules such as HCN, HCl, H_2S, and CH_2CO, are relevant to the sensing of toxic gases and vapors. Heavier molecules are far more challenging for detection because of their large partition functions and more complex spectra,

which tend to merge into broad absorption features at ambient pressure, compromising specificity.

References:

1) M. C. Kemp, P. F. Taday, B. E. Cole, J. A. Cluff, A. J. Fitzgerald, and W. R. Tribe, "Security applications of terahertz technology," Proc. SPIE-Int. Soc. Opt. Eng., **5070**, 44–52 (2003).
2) J. F. Federici, B. Schulkin, F. Huang, D. Gary, R. Barat, F. Oliveira, and D. Zimdars, "THz imaging and sensing for security applications: Explosives, weapons, and drugs," Semicond. Sci. Technol. **20**(7), S266–S280 2005).
3) W. H. Fan, A. Burnett, P. C. Upadhya, J. Cunningham, E. H. Linfield, and A. G. Davies, "Far-infrared spectroscopic characterization of explosives for security applications using broadband terahertz time-domain spectroscopy," Appl. Spectrosc. **61**(6), 638–643 (2007).
4) T. Lo, I. S. Gregory, C. Baker, P. F. Taday, W. R. Tribe, and M. C. Kemp, "The very far-infrared spectra of energetic materials and possible confusion materials using terahertz pulsed spectroscopy," Vib. Spectrosc. **42**(2), 243–248 (2006).
5) J. Chen, Y. Chen, H. Zhao, G. J. Bastiaans, and X.-C. Zhang, "Absorption coefficients of selected explosives and related compounds in the range of 0.1-2.8 THz," Opt. Express **15**(19), 12060–12067 (2007).
6) M. R. Leahy-Hoppa, M. J. Fitch, X. Zheng, L. M. Hayden, and R. Osiander, "Wideband terahertz spectroscopy of explosives," Chem. Phys. Lett. **434**(4-6), 227–230 (2007).
7) J. Wilkinson, C. T. Konek, J. S. Moran, E. M. Witko, and T. M. Korter, "Terahertz absorption spectrum of triacetone triperoxide (TATP)," Chem. Phys. Lett. **478**(4-6), 172–174 (2009).
8) M. van Exter, and D. Grischkowsky, "Characterization of an optoelectronic terahertz beam system," IEEE Trans. Microw. Theory Tech. **38**(11), 1684–1691 (1990).
9) H. Cady, and A. C. Larson, "Pentaerythritol tetranitrate II: its crystal structure and transformation to PETN I; an algorithm for refinement of crystal structures with poor data," Acta Crystallogr. B **31**(7), 1864–1869 (1975).
10) Joseph S. Melinger, S. Sree Harsha, N. Laman and D. Grischkowsky, "Temperature dependent characterization of THz vibrations of explosives and related threat materials," Optics Express, 18, 27238-27250, (2010).
11) Keith C. Oppenheim, Timothy M. Korter, Joseph S. Melinger, and D. Grischkowsky," Solid-state density functional theory investigation of the THz spectra of the structural Isomers 1,2 Dicyanobenzene and 1,3-Dicyanobenzene," J. Phys. Chem. A 2010, 114, 12513-12521, (2010).
12) G.K. Williamson and W.H. Hall, "X-ray line broadening from filed aluminum and wolfram," Acta, Metallurgica 1, 22-31 (1953).
13) N. Laman , S. Sree Harsha, D. Grischkowsky, and Joseph S. Melinger "High-Resolution Waveguide THz Spectroscopy of Biological Molecules", Biophysical Journal, Vol. 94, 1010-1020 (2008).
14) "Substrate independence of THz vibrational modes of polycrystalline thin films of molecular solids in waveguide THz-TDS,", S. Sree Harsha, Joseph. S. Melinger, S. B. Qadri and D. Grischkowsky, J. of Appl. Phys. Lett., 111, 023105, (2012).
15) Sree Harsha Srikantaiah, (2011) " Engineering Metal Parallel Plate Waveguides As a 2-D Plane for High Resolution THz Time Domain Spectroscopy," Ph.D. Thesis, Oklahoma State University.

16) A. Khachatrian, Joseph S. Melinger, and S.B. Qadri, “Waveguide terahertz time-domain spectroscopy of ammonium nitrate polycrystalline films,” J. Appl. Phys. 111, 093103 (2012).
17) M. Theuer, S. Sree Harsha, and D. Grischkowsky, "Flare coupled metal parallel-plate waveguides for high resolution THz time-domain spectroscopy", Journal of Applied Physics, Vol. 108, 113105, (2010).
18) R. Appleby and H. B. Wallace, “Standoff detection of weapons and contraband in the 100 GHz to 1 THz region,” IEEE Trans. Antennas Propag., vol. 55, pp. 2944–2956, Nov. 2007.
19) N. Gopalsami and A. C. Raptis, “Millimeter-wave radar sensing of airborne chemicals,” IEEE Trans. Microw.Theory Tech. **49**(4), 646–653 (2001).
20) H. B. Liu, H. Zhong, N. Karpowicz, Y. Chen, and X.-C. Zhang, “Terahertz Spectroscopy and Imaging for Defense and Security Applications,” Proc. IEEE **95**(8), 1514–1527 (2007).
21) "Measurement of the transmission of the atmosphere from 0.2 to 2 THz ," Yihong Yang, Alisha Shutler, and D. Grischkowsky, Optics Express, 19, 8830-8838, (2011).
22) "Broadband THz Pulse Transmission Through the Atmosphere", Yihong Yang, Mahboubeh Mandehgar, and Daniel R. Grischkowsky, IEEE Trans. Terahertz Science and Technology, 1, No. 1, 264-273, (2011).
23) "THz detection of small molecule vapors in the atmospheric transmission windows," Joseph. S. Melinger, Yihong Yang, Mahboubeh Mandehgar and D. Grischkowsky, Optics Express, 20, pp.6788-6807, (2012).
24) M. Kessler, H. Ring, R. Tramborulo, and W. Gordy, “Microwave spectra and molecular structure of methyl cyanide and isomethyl cyanide,” Phys. Rev. **79**(1), 54–56 (1950).
25) H. M. Pickett, R. L. Poynter, E. A. Cohen, M. L. Delitsky, J. C. Pearson, and H. S. P. Muller, “Sub-millimeter, millimeter, and microwave spectral line catalog,” J. Quant. Spectrosc. Radiat. Transf. **60**(5), 883–890 (1998). Access to specific catalog entries may be found at http://spec.jpl.nasa.gov/

Department Of Defense

Defense Technical Information Center
8725 John J. Kingman Road, Suite 0944
Ft. Belvoir, VA 22060-6201
ATTN: DTIC/OCA

Defense Threat Reduction Information Analysis
Center 8725 John J. Kingman Road, Suite 0944
Ft. Belvoir, VA 22060-6201
ATTN: DTRIAC

Department Of Defense Contractors

Exelis, Inc.
1680 Texas Street, SE
Kirtland AFB, NM 87117-5669
ATTN: DTRIAC

DEPARTMENT OF DEFENSE

DEFENSE THREAT REDUCTION
AGENCY
8725 JOHN J. KINGMAN ROAD
STOP 6201
FORT BELVOIR, VA 22060
ATTN: A. LYALIKOV

DEFENSE TECHNICAL
INFORMATION CENTER
8725 JOHN J. KINGMAN ROAD,
SUITE 0944
FT. BELVOIR, VA 22060-6201
ATTN: DTIC/OCA

DEPARTMENT OF DEFENSE CONTRACTORS

QUANTERION SOLUTIONS, INC.
1680 TEXAS STREET, SE
KIRTLAND AFB, NM 87117-5669
ATTN: DTRIAC